

A Principled Framework for Uncertainty Decomposition in TabPFN

Sandra Fortini ^{*1} Kenyon Ng ^{*2} Sonia Petrone ¹ Judith Rousseau ³ Susan Wei ²

Abstract

TabPFN is a transformer that achieves state-of-the-art performance on supervised tabular tasks by amortizing Bayesian prediction into a single forward pass. However, there is currently no method for **uncertainty decomposition** in TabPFN. Because it behaves, in an idealised limit, as a Bayesian in-context learner, we cast the decomposition challenge as a Bayesian predictive inference (BPI) problem. The main computational tool in BPI, predictive Monte Carlo, is challenging to apply here as it requires simulating unmodeled covariates. We therefore pursue the asymptotic alternative, filling a gap in the theory for supervised settings by proving a predictive CLT under quasi-martingale conditions. We derive variance estimators determined by the volatility of predictive updates along the context. The resulting credible bands are fast to compute, target epistemic uncertainty, and achieve near-nominal frequentist coverage. For classification, we further obtain an entropy-based uncertainty decomposition.

1. Introduction

TabPFN is a foundation transformer model meta-trained on millions of synthetic tabular tasks that can deliver near-instant, state-of-the-art predictions on almost any moderate-sized table via *in-context learning* (Hollmann et al., 2025). It processes a dataset—or *context*—and outputs an approximate posterior predictive distribution (PPD) given a query point in a **single forward pass** of the transformer.

The way in which this efficiency is gained, however, creates a challenge for uncertainty quantification. A rigorous separation of the **aleatoric** and **epistemic** components of total predictive uncertainty in the Bayesian setting typically

^{*}Equal contribution ¹Department of Decision Sciences, Bocconi University, Milan, Italy ²Department of Econometrics and Business Statistics, Monash University, Australia ³CEREMADE, Université Paris Dauphine–PSL, Paris, France and University of Oxford, UK. Correspondence to: Susan Wei <susan.wei@monash.edu>.

Preprint. February 5, 2026.

relies on accessing the posterior distribution. TabPFN, by contrast, *never explicitly represents a posterior distribution*. It treats Bayesian prediction as a direct optimization problem, entirely bypassing the posterior over which one would standardly marginalize to obtain the PPD.

This prediction-first stance points us to a framework known as Bayesian Predictive Inference (BPI) (Fortini & Petrone, 2025) to help meet the challenge of uncertainty decomposition (UD) in TabPFN. BPI is ideally suited for this setting as it inverts the standard Bayesian workflow, treating the predictive rule—rather than the prior-likelihood pair—as the primitive object. Since TabPFN generates this predictive rule directly while maintaining compatibility with Bayesian prediction, it is naturally amenable to the BPI framework.

The BPI framework offers two primary analytical tools: predictive Monte Carlo (MC) and asymptotic approximation. While predictive MC is flexible, it is ill-suited for this setting on both conceptual and computational grounds. Conceptually, it requires simulating future “rollouts,” which in a supervised setting demands a generative model for covariates—something TabPFN does not provide. Computationally, since a single recursive rollout yields only one posterior sample, estimating epistemic uncertainty necessitates generating a large ensemble of such trajectories. This would negate the TabPFN’s primary advantage of near-instant, single-pass inference.

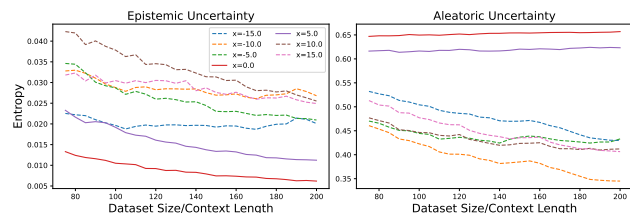


Figure 1. Entropic UD for TabPFN on contexts drawn from logistic regression with different test covariates x against varying context length. Solid and dotted lines indicated in-distribution and out-of-distribution x , respectively. We see decreasing epistemic uncertainty across most x values as context length increases. In addition, the largest epistemic uncertainty occurs at out-of-distribution test covariates while aleatoric uncertainty is highest for $x = 0$ at the decision boundary. See Appendix D for experimental details.

The asymptotic approach is therefore the natural alternative, yet theoretical work in the supervised setting remains

lacking. In particular, existing predictive Central Limit Theorems (CLTs) are limited to unsupervised settings or rely on predictive rules being exchangeable or martingales. Neither set of assumptions is suited to TabPFN, which operates in a supervised setting where the associated predictive rule likely does not strictly satisfy the martingale property.

In this work, we develop a predictive CLT for supervised settings under *quasi-martingale* conditions. We establish a valid estimator for the epistemic variance. The predictive CLT allows us to decompose total predictive uncertainty into aleatoric and epistemic components, applicable to both predictive variance and, through a simple extension, predictive entropy. Figure 1 illustrates the predictive CLT applied to decompose entropic total uncertainty in TabPFN.

Contributions. This work addresses UD in foundation transformer models where the task posterior is implicit. Standard “white-box” methods (e.g., Laplace, SWAG) constitute a category error in this context: they quantify uncertainty in the transformer’s meta-parameters ϕ , rather than the latent task parameters θ . Since TabPFN marginalizes θ directly within the forward pass, task parameters remain inaccessible. We therefore develop a framework grounded in BPI that operates strictly in black-box fashion. Our contributions are:

- **Theoretical Advancement:** We develop a quasi-martingale predictive CLT for supervised regression and classification, deriving explicit variance estimators from the history of predictive updates.
- **Uncertainty Decomposition:** We derive a principled decomposition of total predictive uncertainty into aleatoric and epistemic components, applicable to both predictive variance and predictive entropy.
- **Frequentist Coverage:** We demonstrate that our asymptotic credible bands achieve near-nominal frequentist coverage on simulation benchmarks.

Outline. We review TabPFN and BPI in Section 2. We then present our main methodological contribution – the predictive CLT for supervised settings – and instantiate the framework for TabPFN in Section 3. Section 4 states the formal theorems and assumptions. Section 5 reviews related works. The remaining sections report experiments: we assess frequentist coverage of asymptotic credible bands (Section 6); demonstrate how the predictive CLT can be extended to decompose total entropic predictive uncertainty in classification (Section 7); and compare TabPFN against traditional Bayesian workflows on real data (Section 8).

2. Background

TabPFN. Here we describe the pretraining procedure for TabPFN and why, in an idealised limit, it is a Bayesian in-

context learner. This gives us, at least, conceptual license to use the BPI framework.

TabPFN adopts the meta-learning framework of [Ortega et al. \(2019\)](#), applying it to the specific case of exchangeable tabular data¹. TabPFN implements this framework using a transformer architecture, allowing it to scale to the complexity of the pretraining distribution.

The pretraining corpus consists of a dataset-of-datasets $\{z_{1:n}^m\}_{m=1}^M$, where $z_{1:n}^m = (z_1^m, \dots, z_n^m)$ contains pairs $z_i^m = (x_i^m, y_i^m)$. Each dataset is obtained by first sampling $\theta \sim p(\theta)$ and then drawing samples i.i.d. from the θ -conditional distribution $p_\theta(x, y)$. Crucially, the prior $p(\theta)$ is constructed as a rich mixture of millions of synthetic data-generating processes, primarily consisting of Structural Causal Models and Bayesian Neural Networks.

During meta-training, each dataset $z_{1:n}$ is presented to the transformer as a sequence. At position k , the prefix $z_{1:k-1}$ plays the role of *context* and TabPFN is trained in a next-token fashion to predict the label y_k at covariate x_k . Note that under the generative specification, the conditional distribution of y_k given x_k and the prefix $z_{1:k-1}$ coincides with the **Bayesian posterior predictive distribution** (PPD): $p(y_k \mid x_k, z_{1:k-1}) = \int p_\theta(y_k \mid x_k) p(\theta \mid z_{1:k-1}) d\theta$. In this sense, the training targets are implicitly filtered according to Bayes’ rule: the model sees context–target pairs whose statistics already reflect the Bayesian update, and minimizing log-loss on these Bayes-filtered samples trains TabPFN to approximate, *in context*, the PPD.

TabPFN learns to approximate this PPD by minimizing the negative log-likelihood over the meta-corpus:

$$\frac{1}{M} \sum_{m=1}^M \sum_{i=1}^n -\log q_\phi(y_i^m \mid x_i^m, z_{1:i-1}^m)$$

where q_ϕ is parametrized by a transformer with weights ϕ . In an idealised limit –where training is perfect, M is plentiful so that we approach minimizing the population risk counterpart, and the transformer is sufficiently expressive – the minimizer of this objective is the Bayes PPD. This is the sense in which we mean that TabPFN, in an idealised limit, is a Bayesian in-context learner.

Bayesian predictive inference. We review the framework of Bayesian predictive inference ([Fortini & Petrone, 2025](#)), which underpins our method. The central object here is the sequence of one-step-ahead predictive distributions, analogous to the next-token distributions a transformer defines through in-context learning.

Setup. Let $Z_1, Z_2, \dots \in \mathcal{Z}$ be a stochastic sequence gov-

¹[Ortega et al. \(2019\)](#) originally formulated this for general sequential strategies with the ultimate ambition of approximating Solomonoff induction

erned by a probability law \mathbb{P} . Lower-case $z_{1:n}$ will always denote a concrete realisation of the first n observations. Consider the sequence of one-step-ahead predictive distributions

$$P_n(\cdot) := \mathbb{P}[Z_{n+1} \in \cdot \mid Z_{1:n}], \quad n = 0, 1, 2, \dots,$$

with $P_0(\cdot) = \mathbb{P}[Z_1 \in \cdot]$. We refer to the full sequence $(P_n)_{n \geq 0}$ as a **predictive rule**. Note that each P_n is a predictive distribution for the next observation, and taken together they determine the entire path law \mathbb{P} via the *Ionescu–Tulcea extension theorem* (see [Kallenberg \(2021\)](#) Theorem 5.17 and Corollary 5.18). Conversely, \mathbb{P} determines the predictive rule by conditioning. Thus we may speak interchangeably of the predictive rule $(P_n)_{n \geq 0}$ and the joint law \mathbb{P} it induces.

If $(Z_n)_{n \geq 0}$ is an infinitely **exchangeable** sequence, *de Finetti's Representation theorem* states that there exists a unique probability measure π such that for any n and measurable sets A_1, \dots, A_n ,

$$\mathbb{P}[Z_1 \in A_1, \dots, Z_n \in A_n] = \int \prod_{i=1}^n P(A_i) d\pi(P).$$

where π is the probability law of \tilde{P} . In other words, conditional on the random measure \tilde{P} , the sequence is i.i.d. with distribution \tilde{P} . The random measure \tilde{P} is called the *directing random measure*, and in Bayesian terms it plays the role of the model itself, while its law π acts as the prior over models.

We can relax exchangeability to *asymptotic exchangeability*. This ensures that, for sufficiently large n , a de Finetti-style representation theorem still holds. We say (Z_n) is asymptotically exchangeable with limiting directing random measure \tilde{P} if for $n \rightarrow \infty$, $(Z_{n+1}, Z_{n+2}, \dots) \rightarrow (Z'_1, Z'_2, \dots)$ in distribution where the sequence (Z'_n) is exchangeable with directing random measure \tilde{P} . A sufficient condition for asymptotic exchangeability is that the predictive rule associated to (Z_n) forms a **martingale**. That is, for every measurable $A \subseteq \mathcal{Z}$ and $n \geq 0$:

$$\mathbb{E}[P_{n+1}(A) \mid Z_{1:n}] = P_n(A), \quad \mathbb{P}\text{-a.s.}$$

Once the existence of \tilde{P} is established, we may speak of the object of our focus – the posterior law of $\tilde{P}(A)$ given observed data $z_{1:n}$, for measurable events $A \subseteq \mathcal{Z}$: $\tilde{P}(A) \mid z_{1:n}$. This quantifies how much the predictive distribution is still expected to fluctuate before reaching its asymptote and corresponds to *epistemic* uncertainty (which vanishes as $n \rightarrow \infty$), whereas the uncertainty inherent to \tilde{P} itself constitutes the *aleatoric* uncertainty.

Two general approaches are available in the BPI framework for approximating the posterior law of $\tilde{P}(A)$. We defer discussion of the first approach, which is sampling-based, to Section 5; this approach is computationally expensive

and difficult to extend to supervised settings. In this work we focus on the second approach – a predictive CLT which provides a tractable Gaussian approximation that is fast and avoids explicit modeling of covariates in the supervised setting. We derive a predictive CLT under the weaker quasi-martingale condition that is suitable for regression and classification settings.

3. Methodology

Here we present the predictive CLT result informally; the theorems and assumptions can be found in the following section. Let $Z_i = (X_i, Y_i)$ for $i \geq 1$ be a sequence of observations with $X_i \in \mathcal{X}$ and $Y_i \in \mathcal{Y}$. For any measurable $A \subseteq \mathcal{Y}$, define the predictive probability of A conditional on the history $Z_{1:k}$ and a new covariate x , for $k \geq 0$:

$$P_k(x, A) := \mathbb{P}(Y_{k+1} \in A \mid X_{k+1} = x, Z_{1:k}),$$

with $P_0(x, A) := \mathbb{P}(Y_1 \in A \mid X_1 = x)$. Assume that for any fixed (x, A) , the sequence $(P_k(x, A))_{k \geq 0}$ constitutes a **quasi-martingale**. Under this assumption (and regularity conditions detailed in Section 4), the sequence converges to a limiting random variable $\tilde{P}(x, A)$.

To state the multivariate result, we track m covariate-event pairs $\{(x_j, A_j)\}_{j=1}^m$ and collect their predictive probabilities into the vector $\mathbf{P}_k = (P_k(x_1, A_1), \dots, P_k(x_m, A_m))^{\top}$. Let $\tilde{\mathbf{P}}$ denote the corresponding limiting vector. The predictive CLT states that the posterior distribution of $\tilde{\mathbf{P}}$ is asymptotically Gaussian:

$$\tilde{\mathbf{P}} \mid z_{1:n} \approx \mathcal{N}_m \left(\mathbf{P}_n, \frac{\mathbf{V}_n}{n} \right), \quad (1)$$

where \mathbf{V}_n is the $m \times m$ covariance matrix:

$$\mathbf{V}_n = \frac{1}{n} \sum_{k=1}^n k^2 \mathbf{\Delta}_k \mathbf{\Delta}_k^{\top}, \quad (2)$$

where $\mathbf{\Delta}_k := \mathbf{P}_k - \mathbf{P}_{k-1}$. Note that \mathbf{V}_n is determined by the volatility of the predictive rule's updates along the sequence $z_{1:n}$. Crucially, computing \mathbf{V}_n requires no sampling or imputation of future values; in the case of TabPFN, it relies solely on n forward passes of the transformer.

3.1. Application to Classification and Regression

For binary classification where $\mathcal{Y} = \{0, 1\}$, we focus on the event of a positive label, $A = \{1\}$. We define the sequence of success probabilities as:

$$g_k(x) := P_k(x, \{1\}) = \mathbb{P}[Y_{k+1} = 1 \mid X_{k+1} = x, Z_{1:k}].$$

Our inference target here is the limiting random function

$$\tilde{g}(x) := \tilde{P}(x, \{1\}).$$

For real-valued regression, TabPFN operates by binning the response, effectively reducing regression to multi-class classification. Nonetheless, conceptually we treat the outcome as continuous and focus on events of the type $A_t = (-\infty, t]$. We define the sequence of predictive CDFs as:

$$F_k(x, t) := P_k(x, A_t) = \mathbb{P}[Y_{k+1} \leq t \mid X_{k+1} = x, Z_{1:k}].$$

Our inference target here is the limiting random CDF

$$\tilde{F}(x, t) := \tilde{P}(x, A_t).$$

Let $\{x_1, \dots, x_m\}$ be a grid in the space \mathcal{X} of the covariates, and let $\mathbf{x} = [x_1, \dots, x_m]^T$. For classification, denote the column vectors of predictions and prediction updates

$$\mathbf{g}_n(\mathbf{x}) := (g_n(x_j))_{j=1}^m, \quad \Delta_n(\mathbf{x}) := \mathbf{g}_n(\mathbf{x}) - \mathbf{g}_{n-1}(\mathbf{x}). \quad (3)$$

For regression, let $\mathbf{t} = (t_1, \dots, t_m)$ and similarly denote

$$\begin{aligned} \mathbf{F}_n(\mathbf{x}, \mathbf{t}) &:= (F_n(x_j, t_j))_{j=1}^m, \\ \Delta_n(\mathbf{x}, \mathbf{t}) &:= \mathbf{F}_n(\mathbf{x}, \mathbf{t}) - \mathbf{F}_{n-1}(\mathbf{x}, \mathbf{t}). \end{aligned} \quad (4)$$

Then (1) holds with $\mathbf{P}_n = \mathbf{g}_n$ or $\mathbf{P}_n = \mathbf{F}_n$.

3.2. Uncertainty Decomposition for TabPFN

Let \tilde{P} represent the latent Bayesian model in TabPFN. Our goal is to perform, given $z_{1:n}$, posterior inference for $\tilde{P}(A)$ via the predictive CLT. In what follows, we regard the context $z_{1:n}$ passed into TabPFN as a table where the row is unit of observation and column is feature.

Data Ordering. By design, TabPFN is invariant to *row* permutations meaning the prediction \mathbf{P}_n depends only on the *set* $z_{1:n}$. However, the *trajectory* of updates, e.g., $\mathbf{g}_1, \dots, \mathbf{g}_n$ and $\mathbf{F}_1, \dots, \mathbf{F}_n$, — and thus the asymptotic variance estimator \mathbf{V}_n —depends on the order of the observations. Say in binary classification, if the rows were sorted by class, the early updates would be deceptively small. To recover a representative trajectory that reflects the true epistemic uncertainty of $\tilde{P}(A)$, we randomly permute the rows of $z_{1:n}$ before computing the asymptotic variance.

Computing (2). We construct \mathbf{V}_n by evaluating TabPFN on expanding (non-empty) prefixes of the randomly permuted context. For prefixes that lack diversity we substitute the predictive distribution with the observed statistics: in classification, $g_k(x)$ is set to the constant observed class for single-class prefixes; in regression, $F_k(x, t)$ is set to the marginal empirical CDF of $y_{1:k}$ when fewer than two unique values are present. Otherwise, $g_k(x)$ and $F_k(x, t)$ are obtained via softmax (temperature=1) over the output logits or the discretized bins covering $(-\infty, t]$, respectively.

Computational Efficiency. While computing the asymptotic variance in the predictive CLT requires n forward

passes, this cost must be contextualized within TabPFN’s operational scope – typically small-to-medium tabular datasets (e.g., $n \leq 10,000$). In this regime, the total wall-clock time remains on the order of seconds or minutes. Crucially, this cost is negligible when compared to the methodological alternative that still uses a deep neural network: to achieve comparable uncertainty decomposition without a foundation model, a practitioner would be forced to specify a bespoke Bayesian Neural Network and perform computationally intensive inference (e.g., via MCMC or Variational Inference) for each new dataset. Our framework allows users to extract rigorous epistemic uncertainty estimates directly from the pre-trained TabPFN model via in-context updates, replacing the burdensome tasks of model specification and posterior approximation with a fast procedure.

Asymptotic Validity. Since modern TabPFN variants handle contexts up to $n = 10,000$, we operate well within the regime where asymptotic approximations become reliable. While theoretical finite-sample bounds for this quasi-martingale setting remain open problems, our extensive empirical coverage results (Section 6) demonstrate that the Gaussian approximation holds well even at moderate n .

Ensembling. TabPFN is not invariant to *column* permutations; it natively handles this by averaging predictions over an ensemble of column shuffles (controlled by `n_estimators`). We utilize this built-in mechanism during the computation of the asymptotic variance to ensure the individual predictions for each prefix are stable, thereby reducing the noise in the estimated increments. Unless otherwise specified, we set `n_estimators` = 64.

4. A Predictive CLT for Supervised Settings

We now present the predictive CLT formally. We use the notation $\mathcal{L}(U \mid Z)$ to denote the conditional distribution of a random vector U given a random vector Z . Convergence of probability measures is always understood as weak convergence. All proofs are deferred to Appendix H.

4.1. Convergence of the predictive distributions

Let $Z_n = (X_n, Y_n)$ with $X_n \in \mathcal{X}$ and $Y_n \in \mathcal{Y}$, with \mathcal{X} and \mathcal{Y} being a measurable subset of an Euclidean space and of \mathbb{R} , respectively. Denote by \mathbb{P} the law of (Z_n) . Let $\Delta_n(x, t) = F_n(x, t) - F_{n-1}(x, t)$ be the prediction update based on Z_n . Note that what follows also applies to multi-class classification as long as the type of events we are interested in are atomic or intervals.

Theorem 4.1. *Assume that the following conditions hold:*

- (i) \mathcal{Y} is compact.
- (ii) For every $t \in \mathcal{Y}$, the functions $x \mapsto F_n(x, t)$ are equicontinuous.

(iii) For every x and t ,

$$\sum_{n \geq 1} \mathbb{E}[|\mathbb{E}[\Delta_n(x, t) | Z_{1:n-1}]|] < \infty. \quad (5)$$

Then there exists a kernel $\tilde{F}(x, t)$ such that $F_n(x, \cdot)$ converges weakly to $\tilde{F}(x, \cdot)$ for every $x \in \mathcal{X}$, \mathbb{P} -a.s.

In the literature, when (5) holds $(F_n(x, t))_{n \geq 0}$ is referred to as a **quasi-martingale**. We emphasize that (5) is used here as a sufficient regularity condition to ensure the existence of the limit kernel \tilde{F} ; we do not claim it is necessary. This result can be further strengthened by adding a conditional independence assumption on the covariate process, as stated in the next theorem.

Theorem 4.2. Under the assumption (i)-(iii) of Theorem 4.1 and if:

(iv) For every $n \geq 1$, X_{n+1} is conditionally independent of $Y_{1:n}$, given $X_{1:n}$,

it holds \mathbb{P} -a.s. that the conditional CDF $\mathbb{P}[Y_{n+1} \leq t_1, \dots, Y_{n+k} \leq t_k | X_{n+1:n+k} = x_{1:k}, Z_{1:n}]$ converges weakly to $\prod_{i=1}^k \tilde{F}(x_i, t_i)$ for every x_1, \dots, x_k .

4.2. Asymptotic normality

Since, for every x , $F_n(x, \cdot)$ converges weakly \mathbb{P} -a.s. to $\tilde{F}(x, \cdot)$, then $\mathbf{F}_n(\mathbf{x}, \cdot)$ converges weakly to $\tilde{\mathbf{F}}(\mathbf{x}, \cdot) = [\tilde{F}(x_1, \cdot), \dots, \tilde{F}(x_m, \cdot)]^T$, \mathbb{P} -a.s. In this section, we provide a predictive approximation of $\tilde{\mathbf{F}}(\mathbf{x}, \mathbf{t})$ for fixed \mathbf{x} and \mathbf{t} . Define the matrix of inflated outer product of residuals:

$$\mathbf{R}_n(\mathbf{x}, \mathbf{t}) = n \sum_{k \geq n+1} \mathbf{\Delta}_k(\mathbf{x}, \mathbf{t}) \mathbf{\Delta}_k(\mathbf{x}, \mathbf{t})^T. \quad (6)$$

Theorem 4.3. Let $\mathbf{\Delta}_n(\mathbf{x}, \mathbf{t})$ and $\mathbf{R}_n(\mathbf{x}, \mathbf{t})$ be defined as in (4) and (6), respectively. Under the assumptions of Theorem 4.1, if \mathbf{t} is such that $\mathbf{F}_n(\mathbf{x}, \mathbf{t})$ converges to $\tilde{\mathbf{F}}(\mathbf{x}, \mathbf{t})$ for every \mathbf{x} (\mathbb{P} -a.s.) and the following conditions hold:

(i) For $i = 1, \dots, m$,

$$\sum_{n \geq 1} \sqrt{n} \mathbb{E} \left[|\mathbb{E}[\Delta_n(x_i, t_i) | Z_{1:n-1}]| \right] < \infty; \quad (7)$$

(ii) For $i = 1, \dots, m$, $\mathbb{E} \left[\sup_{n \geq 1} \sqrt{n} |\Delta_n(x_i, t_i)| \right] < \infty$;
(iii) $\mathbf{R}_n(\mathbf{x}, \mathbf{t})$ converges \mathbb{P} -a.s. to a positive definite random matrix $\mathbf{V}(\mathbf{x}, \mathbf{t})$ as $n \rightarrow \infty$.

then

$$\begin{aligned} \mathcal{L}(\sqrt{n}(\mathbf{F}_n(\mathbf{x}, \mathbf{t}) - \tilde{\mathbf{F}}(\mathbf{x}, \mathbf{t})) | Z_{1:n}) \\ \rightarrow \mathcal{N}_m(\mathbf{0}, \mathbf{V}(\mathbf{x}, \mathbf{t})) \quad \mathbb{P}\text{-a.s.} \end{aligned} \quad (8)$$

Under the assumptions of Theorem 4.1, if $\mathbf{F}_n(\mathbf{x}, \cdot)$ is either discrete with fixed support or absolutely continuous with

bounded density, then $\mathbf{F}_n(\mathbf{x}, \mathbf{t})$ converges \mathbb{P} -a.s. to $\tilde{\mathbf{F}}(\mathbf{x}, \mathbf{t})$ for every \mathbf{t} . Note condition (i) of Theorem 4.3 is a stronger version of (5) and is assumed in order to obtain the CLT. We emphasize that (7) is sufficient for our result and is not claimed to be necessary.

On the sufficient conditions. The quasi-martingale condition (5) and the \sqrt{n} -weighted condition (7) are sufficient assumptions used to obtain the convergence and CLT results above. We report empirical diagnostics for TabPFN in Appendix B.

4.3. Asymptotic credible intervals and bands

Let $\mathbf{V}_n(\mathbf{x}, \mathbf{t}) = \frac{1}{n} \sum_{k=1}^n k^2 \mathbf{\Delta}_k(\mathbf{x}, \mathbf{t}) \mathbf{\Delta}_k(\mathbf{x}, \mathbf{t})^T$ and
 $\mathbf{U}_n(\mathbf{x}, \mathbf{t}) = n^2 \mathbb{E} [\mathbf{\Delta}_{n+1}(\mathbf{x}, \mathbf{t}) \mathbf{\Delta}_{n+1}(\mathbf{x}, \mathbf{t})^T | Z_{1:n}]$. (9)

Theorem 4.4. If the following conditions hold:

- (i) For $i = 1, \dots, m$, $\sum_{n \geq 1} n^2 \mathbb{E}[\Delta_n^4(x_i, t_i)] < \infty$;
- (ii) $\mathbf{U}_n(\mathbf{x}, \mathbf{t})$ converges \mathbb{P} -a.s. to a positive definite random matrix $\mathbf{V}(\mathbf{x}, \mathbf{t})$.

then $\mathbf{R}_n(\mathbf{x}, \mathbf{t})$ and $\mathbf{V}_n(\mathbf{x}, \mathbf{t})$ converge to $\mathbf{V}(\mathbf{x}, \mathbf{t})$ \mathbb{P} -a.s. as $n \rightarrow \infty$.

Theorem 4.5. Under the assumptions (i)-(ii) of Theorem 4.3 and (i)-(ii) of Theorem 4.4 with \mathbf{t} such that $\mathbf{F}_n(\mathbf{x}, \mathbf{t})$ converges to $\tilde{\mathbf{F}}(\mathbf{x}, \mathbf{t})$ for every \mathbf{x} , \mathbb{P} -a.s.,

$\mathcal{L}(\sqrt{n} \mathbf{U}_n(\mathbf{x}, \mathbf{t})^{-1/2} (\tilde{\mathbf{F}}(\mathbf{x}, \mathbf{t}) - \mathbf{F}_n(\mathbf{x}, \mathbf{t})) | Z_{1:n}) \rightarrow \mathcal{N}_m(\mathbf{0}, \mathbf{I}_m)$ and

$\mathcal{L}(\sqrt{n} \mathbf{V}_n(\mathbf{x}, \mathbf{t})^{-1/2} (\tilde{\mathbf{F}}(\mathbf{x}, \mathbf{t}) - \mathbf{F}_n(\mathbf{x}, \mathbf{t})) | Z_{1:n}) \rightarrow \mathcal{N}_m(\mathbf{0}, \mathbf{I}_m)$

\mathbb{P} -a.s. as $n \rightarrow \infty$.

While \mathbf{V}_n is computed directly from the observed history, \mathbf{U}_n in (9) requires evaluating an expectation over the next covariate X_{n+1} . We approximate this by sampling X_{n+1} from the empirical measure $\frac{1}{n} \sum_{i=1}^n \delta_{x_i}$. Under the conditions of Theorem 4.4, both \mathbf{V}_n and \mathbf{U}_n serve as valid asymptotic covariance estimators.

Theorem 4.5 and the Portmanteau theorem allow us to construct $(1 - \alpha)$ asymptotic credible sets for the limiting predictive distribution. For the pointwise case ($m = 1$), we obtain intervals:

$$\begin{aligned} I_n^{(1)}(x, t) &= F_n(x, t) \pm z_{1-\alpha/2} \sqrt{n^{-1} U_n(x, t)} \\ I_n^{(2)}(x, t) &= F_n(x, t) \pm z_{1-\alpha/2} \sqrt{n^{-1} V_n(x, t)}, \end{aligned}$$

where $z_{1-\alpha/2}$ is the standard normal $(1 - \alpha/2)$ -quantile. For $j \in \{1, 2\}$, it holds that:

$$\liminf_{n \rightarrow \infty} \mathbb{P} \left[\tilde{F}(x, t) \in I_n^{(j)}(x, t) | Z_{1:n} \right] \geq 1 - \alpha.$$

For the simultaneous case ($m > 1$), we construct credible bands by simulating m -variate Gaussian vectors with covariance \mathbf{C}_n/n , where $\mathbf{C}_n \in \{\mathbf{U}_n, \mathbf{V}_n\}$.

5. Related Work

Meta-learning and approximate Bayesian prediction. The connection between meta-training and approximate Bayesian prediction was articulated by [Ortega et al. \(2019\)](#), who showed that memory-based neural architectures trained to minimize cumulative log-loss on sequences from a generative distribution learn to implement the corresponding Bayesian predictive rule. A growing body of work has since explored this link in increasingly complex settings. [Mikulik et al. \(2020\)](#) study this link in controlled settings by comparing meta-trained agents to Bayes-optimal baselines, and show that meta-training can approximately recover Bayes-optimal behaviour. [Genewein et al. \(2023\)](#) extend this perspective to non-stationary sequence prediction with latent switching structure, demonstrating that modern sequence models (including Transformers) can closely match known Bayes-optimal predictors that marginalize over the latent regime. Finally, [Grau-Moya et al. \(2024\)](#) push the same viewpoint toward increasingly general Bayesian mixture predictors for sequence prediction, up to Solomonoff-style universal prediction. We adopt this shared perspective for TabPFN: meta-training yields an in-context predictor that can be viewed as an approximate Bayesian predictive rule.

Predictive rules used in the BPI framework. BPI has typically been pursued under the assumption that the predictive rule forms a martingale measure; or, in parametric settings, by exploiting the martingale behavior of parameter estimates. However, exact martingale behavior need not hold in practically relevant settings. Notably, [Nagler & Rügamer \(2025\)](#) present a simulation suggesting TabPFN may deviate from the martingale property.²

[Battiston & Cappello \(2025\)](#) relax the martingale property by only requiring that the predictive rule is an almost supermartingale, and show that this elegant property still leads to asymptotic exchangeability of the associated data sequence. Their framework encompasses a wide range of practically relevant procedures, including classical approaches in statistics and learning theory, such as kernel-based estimators, as well as more recent methodologies, such as parametric Bayesian bootstrap schemes.

In this work we take a related perspective, assuming a quasi-martingale property of the predictive probabilities for a fixed event and covariate value. We show that this condition is sufficient for BPI when the response space \mathcal{Y} is compact - an assumption that is natural in many practical applications and, in particular, aligned with TabPFN which bins the response.

Predictive CLTs. Such asymptotic results have been obtained by [Fortini & Petrone \(2020\)](#), [Fortini & Petrone \(2023\)](#)

²The experimental configuration is not fully specified; reproducing the exact setting is therefore nontrivial, so we cite the result primarily as motivation for relaxations beyond martingale.

for martingale predictive rules; [Fong & Yiu \(2024a\)](#) for a general class of parametric martingale posteriors, and [Fong & Yiu \(2024b\)](#) in quantile estimation. These results do not specifically target BPI in supervised learning. Beyond using quasi-martingales, the novelty of our results is in providing predictive CLTs in supervised settings, allowing for predictive inference on the *conditional* distribution of the response given the covariate's values.

Predictive Monte Carlo (MC). As an alternative to asymptotic approximation, we can apply the sampling-based *predictive MC* approach ([Fortini & Petrone, 2020](#)). Predictive MC is valid whenever P_n converges to some \tilde{P} for $n \rightarrow \infty$ and thus is less theoretically demanding to apply than the asymptotic approximation. In predictive MC, we start from the observed data $z_{1:n}$, and for $k = n, \dots, N-1$ simulate $z_{k+1} \sim P_k$. The terminal predictive probability $P_N(A)$ is then treated as one approximate draw from the posterior of $\tilde{P}(A) | z_{1:n}$; repeating this yields many posterior samples³.

Since predictive MC produces posterior draws (of $\tilde{P}(A)$ or functionals of \tilde{P}) without specifying an explicit prior-likelihood pair, it appears tailor-made for uncertainty decomposition for TabPFN. However, in supervised learning, predictive MC must simulate *future covariates* from the predictive rule. TabPFN does not model covariates however—it only provides $\mathbb{P}(Y_{n+1} \in \cdot | X_{n+1} = x, z_{1:n})$. Modelling high-dimensional covariates separately would be burdensome, and the Bayesian-bootstrap workaround suggested by [Fong et al. \(2023\)](#) is, at best, an approximation.

To the best of our knowledge, [Nagler & Rügamer \(2025\)](#) is currently the only work that addresses uncertainty decomposition for TabPFN via predictive MC, but with an important caveat: TabPFN is used only to **initialise** the predictive distribution (their P_0). The subsequent forward simulation proceeds via copula-based updates rather than the predictive rule induced by TabPFN. Consequently, it is unclear whether this constitutes uncertainty decomposition for TabPFN, or rather for a hybrid predictive rule that merely utilises TabPFN for initialisation while relying on standard copulas for the update steps.

Moreover, to circumvent the difficulty of simulating future covariates, [Nagler & Rügamer \(2025\)](#) make uncertainty statements at a single fixed query covariate x^* (e.g., quantiles $\tilde{F}^{-1}(\alpha | x^*)$). Extending their work to many covariate locations is computationally prohibitive, since the predictive MC procedure must be rerun for each x .

UD for transformer-based predictive rules. We provide the first rigorous tool for decomposing total predictive un-

³The same idea underpins the martingale posterior framework of [Fong et al. \(2023\)](#), where it is termed *predictive resampling* and extended to posterior inference for functionals of \tilde{P} , not only the random measure itself.

certainty into aleatoric and epistemic components—using either variance or entropy—for supervised foundation models. While existing documentation suggests TabPFN possesses native uncertainty quantification (PriorLabs, 2025), it only outputs the total posterior predictive distribution, lacking a separate, interpretable notion of epistemic uncertainty. A recent approach by Jayasekera et al. (2025) addresses this for LLMs by optimizing auxiliary queries as probes to bound aleatoric uncertainty. Such variational approximations are necessitated by the fact that LLMs are not explicitly trained to perform Bayesian inference. In contrast, because TabPFN is meta-trained on Bayes-filtered data, its in-context updates naturally approximate a Bayesian predictive rule. This structural property allows us to bypass crude variational bounds and derive a principled decomposition directly from the volatility of the model’s forward passes.

TabPFN for Uncertainty Quantification There is also the tangentially related work of Ng et al. (2025) which uses TabPFN as a predictive engine in martingale posterior. This is not UD for TabPFN but rather TabPFN for UQ in a generalised-Bayes setting. This work nonetheless shares the burden of having to check whether TabPFN satisfies certain theoretical conditions that allow for the BPI framework to be applied. Ng et al. (2025), report that TabPFN does not seem to satisfy the a.c.i.d condition set out in Battiston & Cappello (2025) based on a visual check.

6. Frequentist coverage

A standard diagnostic for Bayesian uncertainty quantification is *frequentist coverage*: under repeated draws of a dataset from a fixed data-generating process (DGP), does a nominal $(1 - \alpha)$ credible set contain the ground truth with probability close to $(1 - \alpha)$? We evaluate coverage at $\alpha = 0.05$ for seven DGPs ; details of the DGPs and evaluation metrics are provided in Appendix F.

Table 1 reports coverage rates and average band widths at various n with two different constructions (Pointwise and Simultaneous) of credible intervals/bands; see Appendix E for the interval/band construction details. Across most DGPs, pointwise intervals achieve coverage exceeding the nominal rate of 0.95 and tighten as n increases, while simultaneous bands are, as expected, wider. The more challenging DGPs (Dependent and Categorical) show the largest deviations from nominal coverage at small n , indicating finite-sample limitations of the Gaussian approximation in these regimes.

The two estimators \mathbf{U}_n and \mathbf{V}_n offer different trade-offs. \mathbf{U}_n is invariant to the ordering of observations within the context, whereas \mathbf{V}_n depends on the specific trajectory of updates. Conversely, \mathbf{V}_n is computed directly from the observed history, while \mathbf{U}_n requires simulating future covariates X_{n+1} . Our simulations do not show a significant covariates

Table 1. Frequentist coverage results for various DGP and sample sizes n for both pointwise and simultaneous credible intervals/bands constructed with either \mathbf{V}_n or \mathbf{U}_n . The nominal coverage targeted is 0.95. In general, we observe that coverage rate increases as n increases while the average width of the credible band decreases. The credible bands produced with \mathbf{U}_n also tend to produce wider credible bands.

DGP	n	\mathbf{V}_n Point.		\mathbf{U}_n Point.		\mathbf{V}_n Simul.		\mathbf{U}_n Simul.	
		Rate	Width	Rate	Width	Rate	Width	Rate	Width
Linear	200	1.00	0.16	0.99	0.18	1.00	0.28	1.00	0.31
	500	1.00	0.13	0.99	0.15	1.00	0.23	1.00	0.26
	1000	1.00	0.12	1.00	0.15	1.00	0.21	1.00	0.26
Polynomial	200	0.99	0.25	1.00	0.28	1.00	0.43	1.00	0.48
	500	0.99	0.19	1.00	0.22	1.00	0.34	0.93	0.39
	1000	1.00	0.17	1.00	0.21	1.00	0.30	1.00	0.36
Dependent	200	0.88	0.26	0.93	0.34	0.73	0.46	0.80	0.57
	500	0.95	0.23	0.96	0.28	0.93	0.41	0.87	0.49
	1000	0.99	0.22	1.00	0.28	1.00	0.38	1.00	0.49
Sine	200	0.98	0.31	1.00	0.36	1.00	0.54	1.00	0.61
	500	0.99	0.25	0.99	0.31	1.00	0.44	1.00	0.53
	1000	1.00	0.23	1.00	0.30	1.00	0.42	1.00	0.53
Poisson	200	0.99	0.74	0.97	0.75	1.00	1.13	1.00	1.17
	500	0.94	0.56	0.94	0.55	1.00	0.90	0.87	0.88
	1000	0.90	0.43	0.90	0.44	1.00	0.71	0.80	0.71
Probit	200	0.97	0.24	0.98	0.27	0.93	0.41	1.00	0.44
	500	0.98	0.20	0.98	0.24	1.00	0.35	0.93	0.41
	1000	0.99	0.18	0.99	0.22	1.00	0.33	1.00	0.37
Categorical	200	0.87	0.26	0.90	0.29	0.53	0.42	0.67	0.48
	500	0.90	0.20	0.94	0.24	0.53	0.35	0.73	0.40
	1000	0.95	0.18	0.96	0.22	0.87	0.32	0.80	0.36

age advantage for \mathbf{U}_n ; however, it is consistently more conservative, yielding wider intervals and bands across nearly all DGPs (Table 1). Given its simplicity, lower computational overhead, and comparable empirical performance, we recommend \mathbf{V}_n for practical UD in TabPFN.

We explicitly omit comparisons to Conformal Prediction (CP) and Deep Ensembles (DE) as they are methodologically misaligned with the objectives of this work. CP provides frequentist coverage guarantees for the total predictive distribution but is inherently “uncertainty-blind” regarding the source; it lacks any mechanism to disentangle epistemic from aleatoric components. Furthermore, CP typically requires a dedicated calibration set, whereas our framework operates purely in-context on a single table. Similarly, DE is a meta-parameter ensemble strategy requiring multiple training runs—an approach that is computationally prohibitive for Foundation Models and fundamentally distinct from our goal of performing uncertainty decomposition on a fixed, pre-trained model via its in-context learning trajectory.

We have an additional set of experiments in Appendix J based on the same 7 DGPs in this section. The goal is not to check coverage but to create “gaps” in the data and see if the estimated epistemic uncertainty is lowest in regions where we have demonstrations and higher as the distance to the in-context data increases. This is inspired by the experiments in Appendix G of Jayasekera et al. (2025).

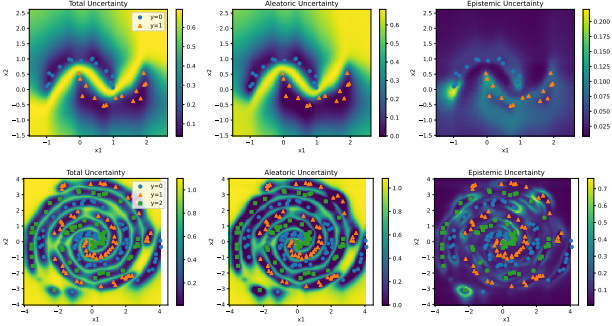


Figure 2. Entropic uncertainty decomposition for two moons (top) and 3-class spirals (bottom) classification tasks. Near the data, the decomposition behaves intuitively: total uncertainty peaks where classes overlap and is correctly attributed to aleatoric uncertainty. In the background regions far from the data, the decomposition diagnoses TabPFN’s tendency to revert to a stable, maximum-entropy prior. Our method faithfully captures this stability as low epistemic uncertainty (reflecting low variance across the ensemble) while assigning the resulting high total entropy to aleatoric uncertainty.

7. Entropy-based uncertainty decomposition.

The predictive CLT can be used as a basis for an entropy-based decomposition of predictive uncertainty for classification tasks. Without loss of generality, we focus on binary classification here; let x^* be a test covariate and $y^* \in \{0, 1\}$ the corresponding label. We measure total predictive uncertainty $U(x^*, z_{1:n})$ by the entropy $\mathbb{H}(y^* | x^*, z_{1:n}) = h(g_n(x^*))$, where $h(p) = -p \log p - (1-p) \log(1-p)$. We follow Jayasekera et al. (2025, Eq. (3)) and decompose total predictive uncertainty as $\mathbb{H}(y^* | x^*, z_{1:n}) = U_a(x^*, z_{1:n}) + U_e(x^*, z_{1:n})$, where $U_a(x^*, z_{1:n}) := \mathbb{E}[h(\tilde{g}(x^*)) | z_{1:n}]$, is aleatoric uncertainty and $U_e(x^*, z_{1:n}) := H(y^* | x^*, z_{1:n}) - U_a(x^*, z_{1:n})$ is epistemic uncertainty.

A straightforward approach is to approximate $U_a(x^*, z_{1:n})$ by a second-order delta-method expansion using the Gaussian approximation for $\tilde{g}(x^*)$ supplied by the predictive CLT. While conceptually simple, this estimate degrades when $g_n(x^*)$ is close to 0 or 1, or when $\frac{v_n(x^*)}{n}$ is sufficiently large. We instead employ a moment-matched Beta approximation. The derivation of \hat{U}_a and the extension to multiclass classification are given in Appendix C.

We illustrate the entropic UD on synthetic experiments. We have already seen a demonstration in Figure 1. Here we show two more experiments on a two-moons dataset and a three-class spiral example in Figure 2. Experimental details and additional results are in Appendix D.

8. Real data illustrations

We illustrate our predictive CLT on a real-data example: the University of Michigan Panel Study of Income Dy-

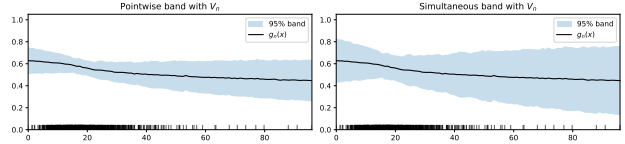


Figure 3. PSID labour-force participation data: TabPFN predicted participation probability $g_n(x)$ versus family income (in \$1000s), with 95% pointwise (left) and simultaneous (right) credible bands. Tick marks indicate observed covariate values.

namics (PSID) labour-force participation dataset studied in Chapter 12.4 of Albert & Hu (2020). The response indicates whether a married woman participates in the labour force, and the covariate is family income excluding her own earnings. The sample size is $n = 753$. The textbook’s canonical Bayesian analysis fits a logistic regression with a conditional-means prior and performs posterior inference via MCMC. Here, we instead apply TabPFN and construct 95% credible bands using predictive CLT.

Figure 3 plots $g_n(x)$ against income with 95% credible bands. The estimated participation probability decreases with income; uncertainty is smallest in the central income range and widens in the tails, with simultaneous bands wider than pointwise bands. The resulting fit is qualitatively similar to the Bayesian logistic regression posterior summaries reported by Albert & Hu (2020), while avoiding explicit prior specification and MCMC. A second real-data illustration on a Bayesian reliability benchmark is in Appendix I.

9. Conclusion

In the idealised limit, TabPFN coincides with an exchangeable Bayesian posterior predictive rule. In practice, TabPFN is a learned approximation, and we currently lack any formal understanding of how closely its in-context updates track a true martingale or Bayesian rule across different tasks.

To accommodate potential deviations from the idealised limit, we therefore work under weaker *sufficient* assumptions—formulated as quasi-martingale conditions—and derive a predictive CLT. We validate the resulting approximation empirically through operational criteria: the asymptotic credible bands constructed from the CLT achieve near-nominal frequentist coverage in our simulated regimes, and the recovered epistemic and aleatoric components behave consistently with the intended decomposition.

We also explored direct diagnostics of the sufficient conditions for the predictive CLT (Appendix B); however, we found the relevant diagnostic quantities rapidly approach the limits of numerical resolution, making high-powered diagnostics computationally demanding. Developing sharper and more efficient diagnostics for stability conditions in black-box BPI predictors such as TabPFN is an important

future direction.

Finally, our predictive CLT is not specific to TabPFN: it applies more broadly to supervised predictive rules within the BPI framework. Natural extensions include fixed-design regression and forms of partial or asymptotic partial exchangeability (e.g., Fortini et al. (2018)).

Acknowledgements

SF and SP were supported by the European Union - Next Generation EU Funds, PRIN 2022 (2022CLTYP4). KN was supported by the Australian Government Research Training Program and the Statistical Society of Australia PhD Top-up Scholarship.

Impact Statement

This paper presents work whose goal is to advance the knowledge of how to do principled uncertainty quantification for Bayesian in-context learners such as TabPFN. There are many potential societal consequences of our work, none which we feel must be specifically highlighted here.

References

Albert, J. and Hu, J. *Probability and Bayesian Modeling*. Texts in Statistical Science. Chapman and Hall/CRC, first edition, 2020.

Battiston, M. and Cappello, L. Bayesian predictive inference beyond martingales. arXiv:2507.21874, 2025.

Berti, P., Crimaldi, I., Pratelli, L., and Rigo, P. A central limit theorem and its applications to multicolor randomly reinforced urns. *Journal of Applied Probability*, 48(2): 527–546, 2011.

Fong, E. and Yiu, A. Asymptotics for parametric martingale posteriors. arXiv:2410.17692, 2024a.

Fong, E. and Yiu, A. Bayesian quantile estimation and regression with martingale posteriors. arXiv:2406.03358, 2024b.

Fong, E., Holmes, C., and Walker, S. G. Martingale posterior distributions. *Journal of the Royal Statistical Society: Series B (Statistical Methodology)*, 85(5):1357–1391, 2023.

Fortini, S. and Petrone, S. Quasi-Bayes properties of a procedure for sequential learning in mixture models. *Journal of the Royal Statistical Society: Series B (Statistical Methodology)*, 82(4):1087–1114, 2020.

Fortini, S. and Petrone, S. Prediction-based uncertainty quantification for exchangeable sequences. *Philosophical Transactions of the Royal Society A: Mathematical, Physical and Engineering Sciences*, 381(2247), 2023.

Fortini, S. and Petrone, S. Exchangeability, prediction and predictive modeling in Bayesian statistics. *Statistical Science*, 40(1):40–67, 2025.

Fortini, S., Petrone, S., and Sporysheva, P. On a notion of partially conditionally identically distributed sequences. *Stochastic Processes and their Applications*, 128(3):819–846, 2018.

Genewein, T., Deletang, G., Ruoss, A., Wenliang, L. K., Catt, E., Dutordoir, V., Grau-Moya, J., Orseau, L., Hutter, M., and Veness, J. Memory-based meta-learning on non-stationary distributions. In *Proceedings of the International Conference on Machine Learning*, pp. 11173–11195, 2023.

Grau-Moya, J., Genewein, T., Hutter, M., Orseau, L., Deletang, G., Catt, E., Ruoss, A., Wenliang, L. K., Mattern, C., Aitchison, M., and Veness, J. Learning universal predictors. In *Proceedings of the International Conference on Machine Learning*, pp. 16178–16205, 2024.

Hamada, M. S., Wilson, A. G., Reese, C. S., and Martz, H. F. *Bayesian Reliability*. Springer Series in Statistics. Springer, 2008.

Hollmann, N., Müller, S., Purucker, L., Krishnakumar, A., Körfer, M., Hoo, S. B., Schirrmeister, R. T., and Hutter, F. Accurate predictions on small data with a tabular foundation model. *Nature*, 637(8045):319–326, 2025.

Jayasekera, I. S., Si, J., Valdettaro, F., Chen, W., Faisal, A. A., and Li, Y. Variational uncertainty decomposition for in-context learning. In *Advances in Neural Information Processing Systems*, 2025.

Kallenberg, O. *Foundations of Modern Probability*, volume 99 of *Probability Theory and Stochastic Modelling*. Springer International Publishing, 2021.

Mikulik, V., Delétang, G., McGrath, T., Genewein, T., Martic, M., Legg, S., and Ortega, P. Meta-trained agents implement Bayes-optimal agents. In *Advances in Neural Information Processing Systems*, volume 33, pp. 18691–18703, 2020.

Nagler, T. and Rügamer, D. Uncertainty quantification for prior-data fitted networks using martingale posteriors. arXiv:2505.11325, 2025.

Ng, K., Fong, E., Frazier, D. T., Knoblauch, J., and Wei, S. TabMGP: Martingale posterior with TabPFN. arXiv:2510.25154, 2025.

Olea, J. L. M. and Plagborg-Møller, M. Simultaneous confidence bands: Theory, implementation, and an application to SVARs. *Journal of Applied Econometrics*, 34(1):1–17, 2019.

Ortega, P. A., Wang, J. X., Rowland, M., Genewein, T., Kurth-Nelson, Z., Pascanu, R., Heess, N., Veness, J., Pritzel, A., Sprechmann, P., Jayakumar, S. M., McGrath, T., Miller, K., Azar, M., Osband, I., Rabinowitz, N., György, A., Chiappa, S., Osindero, S., Teh, Y. W., van Hasselt, H., de Freitas, N., Botvinick, M., and Legg, S. Meta-learning of Sequential Strategies. arXiv:1905.03030, 2019.

PriorLabs. TabPFN documentation: Intended use. https://priorlabs.ai/getting_started/intended_use/#computational-and-time-requirements, 2025.

A. Experiment code and default settings

The code is released at <https://anonymous.4open.science/r/ud4pfn-B017>.

Throughout, we set `n_estimators=64`, unless stated otherwise. We also set `softmax_temperature=1.0` and use the default initialisation settings in `tabPFN==6.2.0`. We use `tabPFN-v2.5-classifier-v2.5_default.ckpt` for `TabPFNClassifier` and `tabPFN-v2.5-classifier-v2.5_default.ckpt` for `TabPFNRegressor`. The checkpoints were downloaded from https://huggingface.co/Prior-Labs/tabPFN_2_5/tree/main.

B. Diagnostics for Predictive CLT sufficient conditions in TabPFN

We empirically assess whether the theoretical conditions required for the predictive CLT (Section 4) are plausibly satisfied by TabPFN. The assumptions in our theorems are asymptotic and involve expectations taken over the path of the predictive rule. Since TabPFN is a black-box function, these conditions cannot be formally verified; instead, we perform diagnostics to detect *gross violations* in a controlled setting.

To make the large number of TabPFN refits computationally feasible, we use a smaller ensemble size (`n_estimators=8` and `16`) than in the other experiments in this paper.

We focus on three key conditions:

- the quasi-martingale condition (5) (condition (iii) of Theorem 4.1),
- the stronger \sqrt{n} -weighted quasi-martingale property (7) (condition (i) of Theorem 4.3), and
- the normalization of \mathbf{U}_n .

B.1. Quantities appearing in the conditions

Fix a single query covariate $x^* = 1$ and define the increment at the query point

$$\Delta_n = g_n(x^*) - g_{n-1}(x^*),$$

where

$$g_n(x) = \mathbb{P}(Y = 1 \mid X = x, Z_{1:n}).$$

Define the conditional first and second moments

$$b_n = \mathbb{E}[\Delta_n \mid Z_{1:n-1}], \quad b'_n = \mathbb{E}[\Delta_n^2 \mid Z_{1:n-1}].$$

The sufficient conditions in Section 4 reduce (in this scalar setup) to summability of the expected absolute conditional drift,

$$\sum_{n \geq 1} \mathbb{E}|b_n| < \infty \quad \text{and} \quad \sum_{n \geq 1} \sqrt{n} \mathbb{E}|b_n| < \infty.$$

We also check whether $n^2 b'_n$ is approximately constant in the tail, which corresponds to the n^2 normalization used in \mathbf{U}_n .

To summarize tail behaviour, we use power-law fits:

$$\mathbb{E}|b_n| \approx Cn^{-\beta}, \quad b'_n \approx Cn^{-\gamma}.$$

Under a clean power-law model, the unweighted and weighted summability conditions correspond heuristically to $\beta > 1$ and $\beta > 1.5$, and $\gamma \approx 2$ corresponds to b'_n behaving like n^{-2} (consistent with the $n^2 b'_n$ scaling).

B.2. Computing b_n and b'_n given a prefix (exact inner expectation)

To reduce Monte Carlo variability, we use a discrete covariate distribution:

$$X_i \in \{-1, 0, 1, 2\}, \quad \mathbb{P}(X_i = x) = \frac{1}{4},$$

and binary outcomes $Y_i \in \{0, 1\}$. In this setting, the conditional expectations over (X_n, Y_n) can be computed *exactly* for each prefix $Z_{1:n-1}$ (no simulation inside the conditional expectation).

Let the support points be $x^{(j)} \in \{-1, 0, 1, 2\}$. For a fixed prefix $Z_{1:n-1}$:

1. Fit TabPFN on $Z_{1:n-1}$ and compute $g_{n-1}(x^*)$ and $g_{n-1}(x^{(j)})$ for each j .

2. For each j , refit TabPFN on the two augmented prefixes

$$Z_{1:n-1} \cup \{(x^{(j)}, 0)\}, \quad Z_{1:n-1} \cup \{(x^{(j)}, 1)\},$$

and evaluate the resulting next-step predictions at the query point x^* :

$$g_n^{(j,0)}(x^*) \equiv \mathbb{P}(Y_{n+1} = 1 \mid X_{n+1} = x^*, Z_{1:n-1}, Z_n = (x^{(j)}, 0)),$$

$$g_n^{(j,1)}(x^*) \equiv \mathbb{P}(Y_{n+1} = 1 \mid X_{n+1} = x^*, Z_{1:n-1}, Z_n = (x^{(j)}, 1)).$$

3. Define $d_0^{(j)} = g_n^{(j,0)}(x^*) - g_{n-1}(x^*)$ and $d_1^{(j)} = g_n^{(j,1)}(x^*) - g_{n-1}(x^*)$.

4. Average over $Y_n \in \{0, 1\}$ conditional on $X_n = x^{(j)}$:

$$\mathbb{E}[\Delta_n \mid Z_{1:n-1}, X_n = x^{(j)}] = (1 - g_{n-1}(x^{(j)}))d_0^{(j)} + g_{n-1}(x^{(j)})d_1^{(j)},$$

$$\mathbb{E}[\Delta_n^2 \mid Z_{1:n-1}, X_n = x^{(j)}] = (1 - g_{n-1}(x^{(j)}))(d_0^{(j)})^2 + g_{n-1}(x^{(j)})(d_1^{(j)})^2.$$

5. Finally, average over the covariate law (independent of the prefix, consistent with Theorem 4.2(iv)):

$$b_n = \sum_j \frac{1}{4} \mathbb{E}[\Delta_n \mid Z_{1:n-1}, X_n = x^{(j)}], \quad b'_n = \sum_j \frac{1}{4} \mathbb{E}[\Delta_n^2 \mid Z_{1:n-1}, X_n = x^{(j)}].$$

B.3. TabPFN-induced rollouts (how prefixes are generated)

Each *rollout* is a synthetic sequence produced by iterating the TabPFN one-step predictive rule.

Initial context. We first generate $n_0 = 25$ observations under a simple logistic model:

$$\mathbb{P}(Y_i = 1 \mid X_i = x) = \sigma(\beta x + \beta_0), \quad \sigma(u) = \frac{1}{1 + e^{-u}},$$

with $\beta = 2.0$ and $\beta_0 = -0.5$, and X_i drawn i.i.d. from the discrete covariate law above. We ensure the initial prefix contains both label classes; if not, we resample the initial context.

Rollout. After the initial context generated from the DGP, we extend the sequence to $N_{\text{end}} = n_0 + 1000$ by sampling future data according to the TabPFN-induced predictive rule. For each $t = n_0 + 1, \dots, N_{\text{end}}$:

1. Draw X_t i.i.d. from $\{-1, 0, 1, 2\}$ with mass $1/4$.
2. Fit TabPFN on $Z_{1:t-1}$ and compute $g_{t-1}(X_t) = \mathbb{P}(Y_t = 1 \mid X_t, Z_{1:t-1})$.
3. Sample $Y_t \sim \text{Bernoulli}(g_{t-1}(X_t))$.

If a prefix contains only one label class, we do not call TabPFN and instead set $g_{t-1}(x)$ to the corresponding degenerate value (0 or 1) until both classes are present.

B.4. Estimation protocol (replicates, tail grid, and fits)

Across-rollout averaging. The conditional quantities b_n and b'_n depend on the realized prefix $Z_{1:n-1}$. We approximate $\mathbb{E}|b_n|$ by averaging over $R = 100$ independent rollouts:

$$\widehat{\mathbb{E}}|b_n| = \frac{1}{R} \sum_{r=1}^R |b_n^{(r)}|.$$

Tail grid. Each rollout extends to $N_{\text{end}} = n_0 + 1000$, but we evaluate conditional moments only on a sparse *tail grid*: $m_{\text{tail}} = 100$ geometrically spaced prefix lengths between $N_{\text{start}} = n_0 + 100$ and N_{end} , rounded to integers.

Power-law summaries. We fit

$$\hat{\mathbb{E}}|b_n| \approx Cn^{-\beta}$$

by ordinary least squares on log–log axes over the tail grid, and report a 95% confidence interval for the slope based on the standard error in log space. For the conditional second moment, we fit per-rollout exponents

$$b_n'^{(r)} \approx C_r n^{-\gamma_r}$$

and summarize across rollouts by the median exponent $\hat{\gamma}_{\text{med}}$. To visualize the implied normalization, we plot $n^{\hat{\gamma}_{\text{med}}} b_n'^{(r)}$ (and its across-rollout mean) over the tail grid.

Partial-sum diagnostics. We additionally consider cumulative diagnostics

$$S(n) = \sum_{n_0 \leq m \leq n} \mathbb{E}|b_m|, \quad T(n) = \sum_{n_0 \leq m \leq n} \sqrt{m} \mathbb{E}|b_m|.$$

Due to computational constraints, we evaluate $\mathbb{E}|b_m|$ on the tail grid and approximate these sums by trapezoidal block rules. We also evaluate every fifth term between n_0 and $n_0 + 100$ to better capture the early part of the sum.

B.5. Findings

Normalization of \mathbf{U}_n . Across rollouts, the fitted tail exponents for the conditional second moment concentrate near 2 (Figures 4 and 5), with $\hat{\gamma}_{\text{med}} \approx 2$. The rescaled curves $n^{\hat{\gamma}_{\text{med}}} b_n'^{(r)}$ are relatively stable in the tail (Figure 6). Interpreting b_n' as the typical squared one-step update at the query point, this behaviour is consistent with b_n' decaying approximately like n^{-2} , supporting the use of an n^2 scaling in \mathbf{U}_n in this controlled setting.

Quasi-martingale and \sqrt{n} -weighted conditions. Figure 7 shows $\hat{\mathbb{E}}|b_n|$ together with the fitted power law on log–log axes. For $n_{\text{estimators}} = 8$ and 16, the fitted decay rates are $\hat{\beta} \approx 0.87$ (95% CI [0.77, 0.98]) and $\hat{\beta} \approx 0.73$ (95% CI [0.67, 0.80]), respectively. Under a clean power-law model, the unweighted and weighted summability conditions correspond to $\beta > 1$ and $\beta > 1.5$, respectively. In the far tail, $\hat{\mathbb{E}}|b_n|$ approaches numerical/Monte Carlo precision limits, so tail slope estimates are sensitive to the evaluation range. For context, Figures 8 and 9 plot the cumulative sums $S(n)$ and $T(n)$ over the probed range; we do not see behaviour consistent with $\beta > 1.5$ under this diagnostic, while the unweighted behaviour is harder to distinguish from the numerical/Monte Carlo floor. We emphasize that (7) is a sufficient condition used to obtain the CLT in Section 4.

Computational limitations. These checks require repeated TabPFN refits on many prefixes and many augmented prefixes, which limits both the number of rollouts and the tail depth that can be explored. Developing diagnostics that remain informative at practical compute budgets—especially in the near-martingale regime where update magnitudes approach numerical precision—is an important direction for future work.

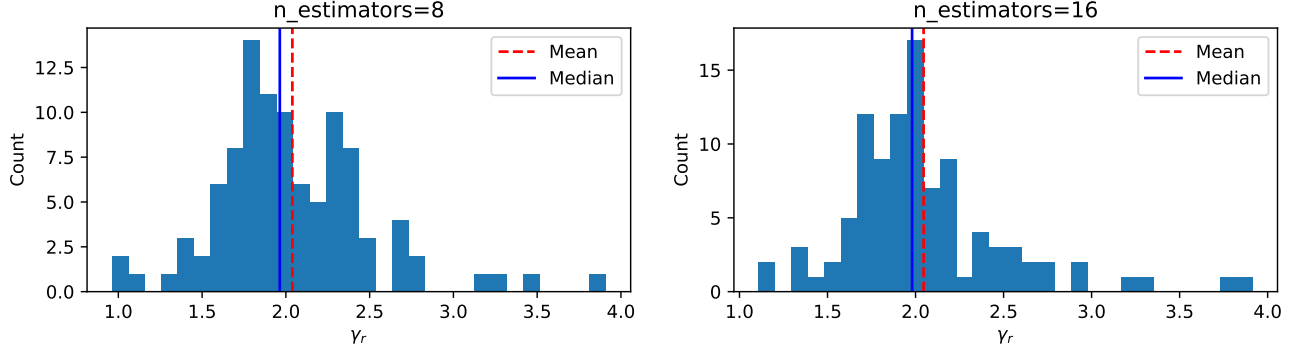


Figure 4. (γ_r summary) A histogram of the fitted γ_r over 100 rollouts. The TabPFN ensemble size is 8 (left) and 16 (right).

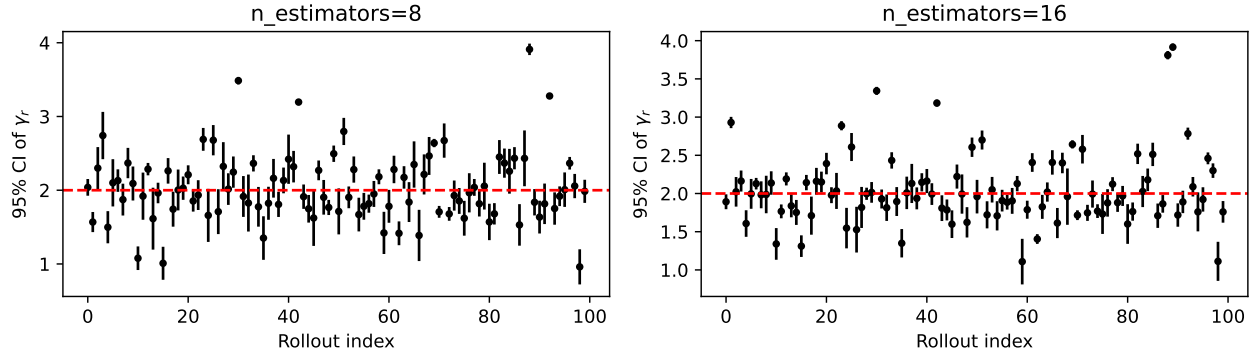


Figure 5. (γ_r summary) 95% confidence intervals of the fitted γ_r over 100 rollouts. Ideally, the intervals should contain 2 (red dotted line). The TabPFN ensemble size is 8 (left) and 16 (right).

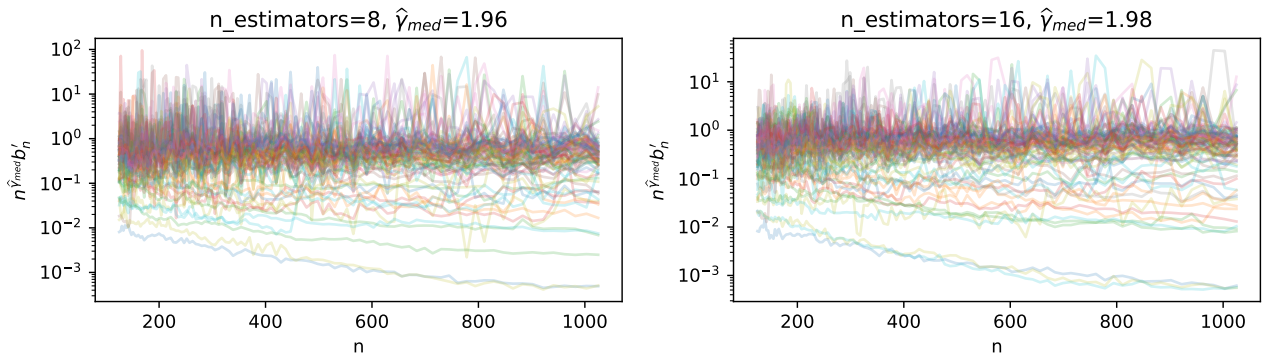


Figure 6. (Scaled b'_n) Each coloured curve represents the trajectory $n \hat{\gamma}_{med} b'^{(r)}_n$ from a rollout. Ideally, each trajectory should remain constant as n increases. The TabPFN ensemble size is 8 (left) and 16 (right).

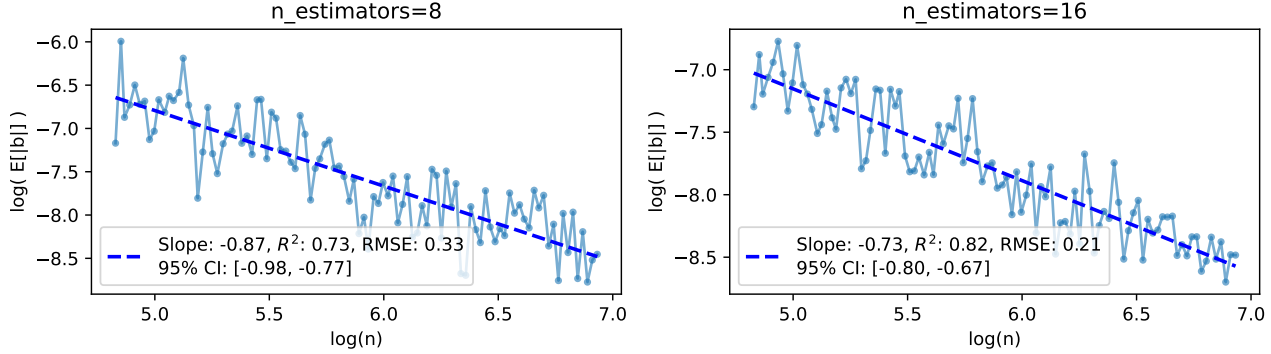


Figure 7. (Mean drift magnitude) The across-rollout mean $\widehat{\mathbb{E}}|b_n|$ with its fitted power law $Cn^{-\widehat{\beta}}$, shown on log–log axes. The fitted $\widehat{\beta}$ are 0.87 and 0.73 for ensemble sizes 8 and 16, respectively.

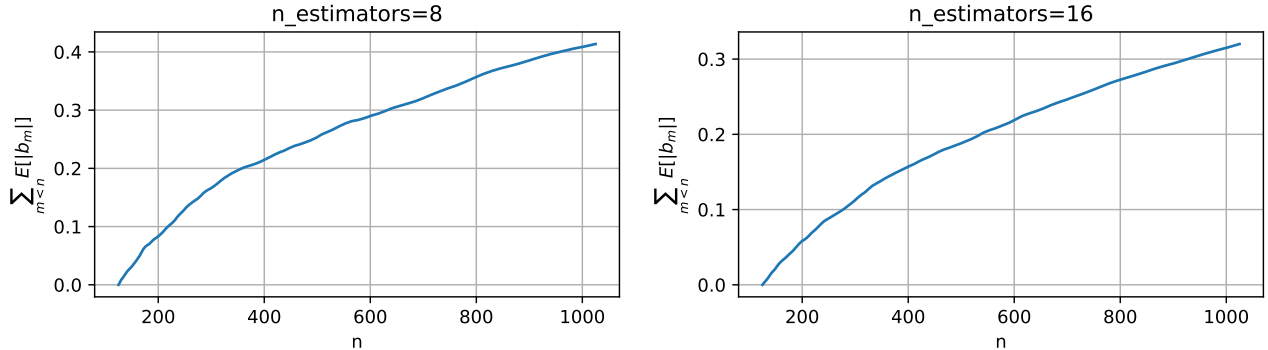


Figure 8. (Partial-sum diagnostics) The partial sum $\sum_{m< n} \mathbb{E}[|b_m|]$ as n increases. Ideally, the curve should flatten out as $n \rightarrow \infty$. The TabPFN ensemble size is 8 (left) and 16 (right).

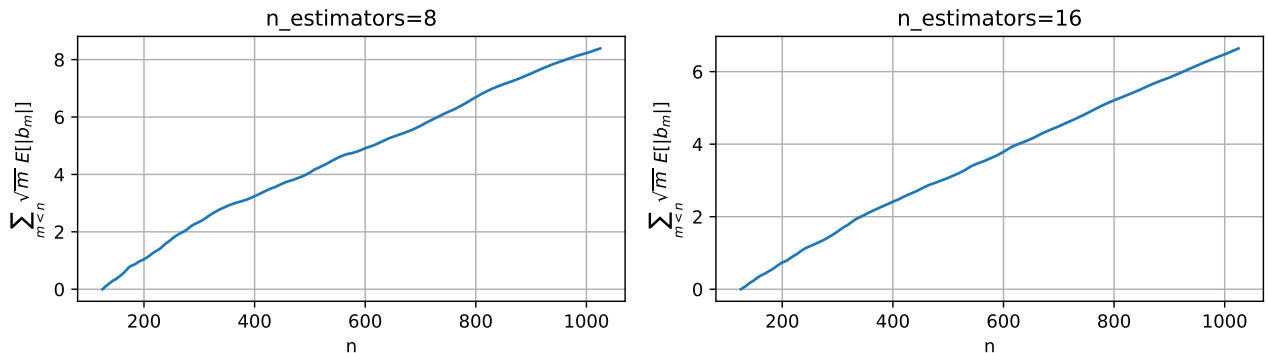


Figure 9. (Partial-sum diagnostics) The partial sum $\sum_{m< n} \sqrt{m} \mathbb{E}[|b_m|]$ as n increases. Ideally, the curve should flatten out as $n \rightarrow \infty$. The TabPFN ensemble size is 8 (left) and 16 (right).

C. Derivations for entropy-based uncertainty decomposition

Fix a test point x^* . Our goal is to approximate the aleatoric uncertainty component:

$$U_a(x^*, z_{1:n}) = \mathbb{E}[h(\tilde{g}(x^*)) \mid z_{1:n}],$$

where $h(p) = -p \log p - (1-p) \log(1-p)$ is the binary entropy function. The Gaussian approximation provided by the predictive CLT, $\tilde{g}(x^*) \mid z_{1:n} \approx \mathcal{N}(g_n(x^*), v_n(x^*)/n)$, does not respect the support constraint $\tilde{g}(x^*) \in [0, 1]$ and is therefore unsuitable for directly computing the expectation of the entropy.

We first preview the result before giving the derivation. Concretely, define the (clipped) plug-in variance

$$\sigma_n^2(x^*) := \min \left\{ \frac{v_n(x^*)}{n}, g_n(x^*)(1 - g_n(x^*)) \right\}.$$

Then set

$$T_n(x^*) := \frac{g_n(x^*)(1 - g_n(x^*))}{\sigma_n^2(x^*)} - 1,$$

and define

$$\alpha_n(x^*) := g_n(x^*) T_n(x^*)$$

and

$$\beta_n(x^*) := (1 - g_n(x^*)) T_n(x^*).$$

For $g_n(x^*) \in (0, 1)$ and $T_n(x^*) > 0$, $\text{Beta}(\alpha_n(x^*), \beta_n(x^*))$ has mean $g_n(x^*)$ and variance $\sigma_n^2(x^*)$. Let ψ denote the digamma function. Our estimator of aleatoric (entropic) uncertainty at x^* is

$$\widehat{U}_a(x^*, z_{1:n}) := -\frac{\alpha_n(x^*)}{\alpha_n(x^*) + \beta_n(x^*)} \psi(\alpha_n(x^*) + 1) - \frac{\beta_n(x^*)}{\alpha_n(x^*) + \beta_n(x^*)} \psi(\beta_n(x^*) + 1) + \psi(\alpha_n(x^*) + \beta_n(x^*) + 1). \quad (10)$$

C.1. Moment-matched Beta approximation

To enforce the support constraint, we approximate the posterior of $\tilde{g}(x^*)$ by a Beta distribution, denoted by $G \sim \text{Beta}(\alpha_n, \beta_n)$. We determine the parameters α_n and β_n by matching the first two moments of G to the mean and variance given by the CLT:

$$\begin{aligned} \mathbb{E}[G] &= \frac{\alpha_n}{\alpha_n + \beta_n} = g_n(x^*), \\ \text{Var}(G) &= \frac{\alpha_n \beta_n}{(\alpha_n + \beta_n)^2 (\alpha_n + \beta_n + 1)} = \frac{v_n(x^*)}{n}. \end{aligned}$$

Solving this system for α_n and β_n yields:

$$\alpha_n = g_n(x^*) T_n(x^*), \quad (11)$$

$$\beta_n = (1 - g_n(x^*)) T_n(x^*), \quad (12)$$

where

$$T_n(x^*) = \frac{g_n(x^*)(1 - g_n(x^*))}{v_n(x^*)/n} - 1.$$

We clip the plug-in variance $v_n(x^*)/n$ to be strictly less than $g_n(x^*)(1 - g_n(x^*))$ to ensure $T_n(x^*) > 0$.

Using standard properties of the Beta distribution, the expected entropy $\mathbb{E}[h(G)]$ can be expressed in terms of digamma functions $\psi(\cdot)$. Specifically, we have $\mathbb{E}[\log G] = \psi(\alpha_n) - \psi(\alpha_n + \beta_n)$ and $\mathbb{E}[\log(1 - G)] = \psi(\beta_n) - \psi(\alpha_n + \beta_n)$. Substituting these into the definition of entropy yields the closed-form estimator $\widehat{U}_a(x^*, z_{1:n})$.

C.2. Comparison with Delta method

A simpler alternative would be a second-order Delta method expansion around the mean $g_n(x^*)$. Since $h''(p) = -1/(p(1-p))$, this yields:

$$U_a(x^*, z_{1:n}) \approx h(g_n(x^*)) - \frac{v_n(x^*)/n}{2g_n(x^*)(1-g_n(x^*))}. \quad (13)$$

However, this approximation is numerically unstable near the boundaries (where $g_n(x^*) \approx 0$ or 1), as the curvature h'' explodes. Furthermore, this approximation is not guaranteed to be bounded by the total entropy $h(g_n(x^*))$, potentially leading to negative estimates for the epistemic uncertainty $U_e(x^*, z_{1:n})$. The moment-matched Beta approach avoids these pathologies by implicitly respecting the compact support of $\tilde{g}(x^*)$.

C.3. Extension to multiclass classification

For the multiclass setting with K classes, let the predictive distribution be denoted by the probability vector $g_n(x^*) = [g_{n,1}(x^*), \dots, g_{n,K}(x^*)]^\top$, where $\sum_{k=1}^K g_{n,k}(x^*) = 1$. The total predictive uncertainty is given by the Shannon entropy:

$$\mathbb{H}(y^* \mid x^*, z_{1:n}) = - \sum_{k=1}^K g_{n,k}(x^*) \log g_{n,k}(x^*). \quad (14)$$

We decompose this into aleatoric and epistemic components. To estimate the aleatoric uncertainty $U_a(x^*, z_{1:n})$, we generalize the Beta approximation to a Dirichlet approximation $\tilde{g}(x^*) \sim \text{Dir}(\alpha_n(x^*))$, where $\alpha_n(x^*) = [\alpha_{n,1}(x^*), \dots, \alpha_{n,K}(x^*)]^\top$.

We determine the parameters via moment matching. Let $\sigma_{n,k}^2(x^*)$ denote the variance for class k provided by the predictive CLT, analogous to the binary case. We define the term $\alpha_{n,0}(x^*)$ by matching the total variance of the Dirichlet distribution to the sum of the predictive variances:

$$\sum_{k=1}^K \frac{g_n(x^*)(1-g_n(x^*))}{\alpha_{n,0}(x^*) + 1} = \sum_{k=1}^K \sigma_{n,k}^2(x^*). \quad (15)$$

Rearranging the terms yields

$$\alpha_{n,0}(x^*) := \frac{1 - \|g_n(x^*)\|_2^2}{\sum_{k=1}^K \sigma_{n,k}^2(x^*)} - 1. \quad (16)$$

The sum of the predictive variances $\sum_{k=1}^K \sigma_{n,k}^2(x^*)$ is clipped to be strictly less than $1 - \|g_n(x^*)\|_2^2$ to ensure $\alpha_{n,0}(x^*) > 0$. The Dirichlet parameters are then set as $\alpha_{n,k}(x^*) := g_{n,k}(x^*) \alpha_{n,0}(x^*)$.

The aleatoric uncertainty is estimated as the expected entropy of this Dirichlet distribution. Using the properties of the digamma function ψ , we obtain the estimator:

$$\widehat{U}_a(x^*, z_{1:n}) := \psi(\alpha_{n,0}(x^*) + 1) - \sum_{k=1}^K g_{n,k}(x^*) \psi(\alpha_{n,k}(x^*) + 1). \quad (17)$$

Epistemic uncertainty is then computed as the residual $U_e(x^*, z_{1:n}) = \mathbb{H}(y^* \mid x^*, z_{1:n}) - \widehat{U}_a(x^*, z_{1:n})$.

D. Entropic uncertainty decomposition experiments

We take the synthetic experimental setups described in Jayasekera et al. (2025), Appendix G.3 (“Synthetic Toy Experiments”), including the data-generating processes and evaluation grids for logistic regression, Two Moons, and Spirals.

D.1. Logistic regression (1D)

We consider a one-dimensional logistic-regression data-generating process. For each dataset size n , we sample covariates $x_i \sim \mathcal{N}(1.5, 3.0^2)$ and then draw labels

$$y_i \sim \text{Bernoulli}(p_i), \quad p_i = \sigma(\beta x_i + \beta_0),$$

where $\sigma(\cdot)$ is the logistic sigmoid, $\beta = 0.25$, and $\beta_0 = -0.5$. We run this experiment for $n \in \{15, 50, 75, 150\}$ with a fixed random seed.

For visualization, we evaluate uncertainty on a one-dimensional test grid $x^* \in [-15.0, 15.0]$ with step size 0.2. The results are in Figure 10.

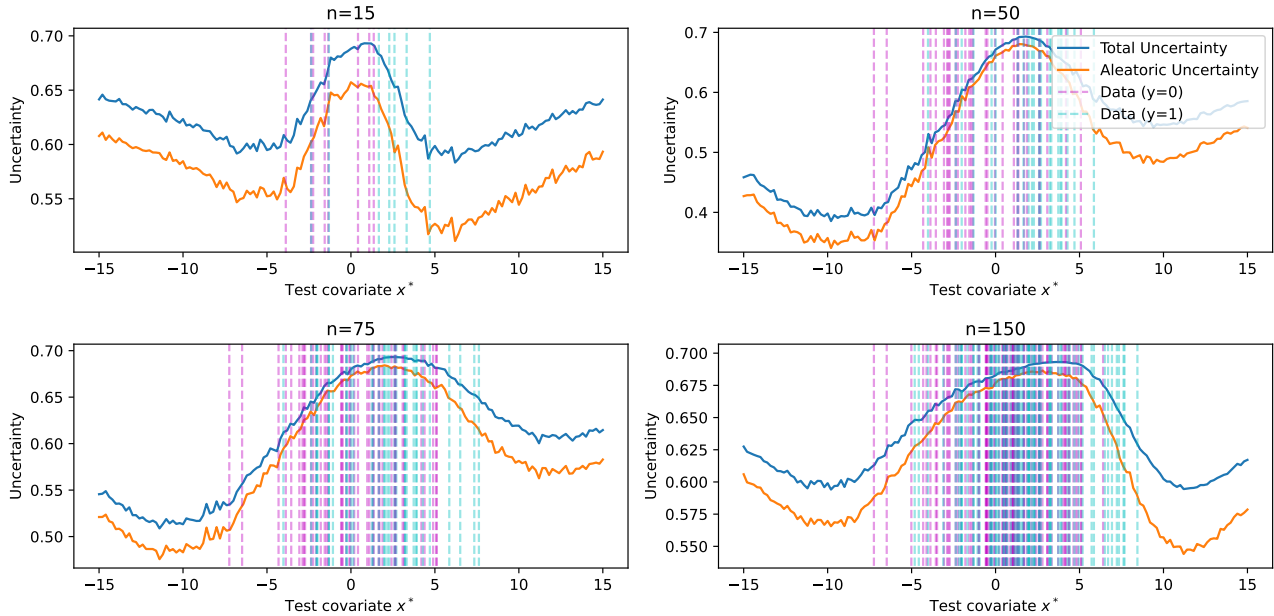


Figure 10. Logistic regression (1D). Entropy-based uncertainty decomposition for TabPFN at dataset sizes $n \in \{15, 50, 75, 150\}$.

Size curves. To study scaling with dataset size, we evaluate uncertainties at test points $x^* \in \{-15, -10, -5, 0, 5, 10, 15\}$ across dataset sizes $n \in \{75, 80, 85, \dots, 200\}$. For each size n , we average results across $R = 50$ independently sampled datasets. The raw values of the aleatoric and epistemic uncertainty are presented in Figure 1. In addition, we also show the aleatoric and epistemic uncertainty as a proportion of the total uncertainty in Figure 11.

D.2. Two Moons (binary classification)

We use the `scikit-learn make_moons` generator with additive Gaussian noise. We consider two noise regimes: (i) *Moons 1* with noise $\sigma = 0.1$ and (ii) *Moons 2* with noise $\sigma = 0.4$. For each regime we run two dataset sizes, $n = 30$ and $n = 100$, using a fixed seed. We evaluate uncertainty on two-dimensional uniform grids with 100 points in each coordinate:

- **Moons 1:** $x_1^* \in [-1.5, 2.5]$ and $x_2^* \in [-1.5, 2.5]$.
- **Moons 2:** $x_1^* \in [-3.0, 3.5]$ and $x_2^* \in [-2.5, 3.0]$.

We report heatmaps of total, aleatoric, and epistemic uncertainty over each grid, overlaying training samples by class, see Figures 12.

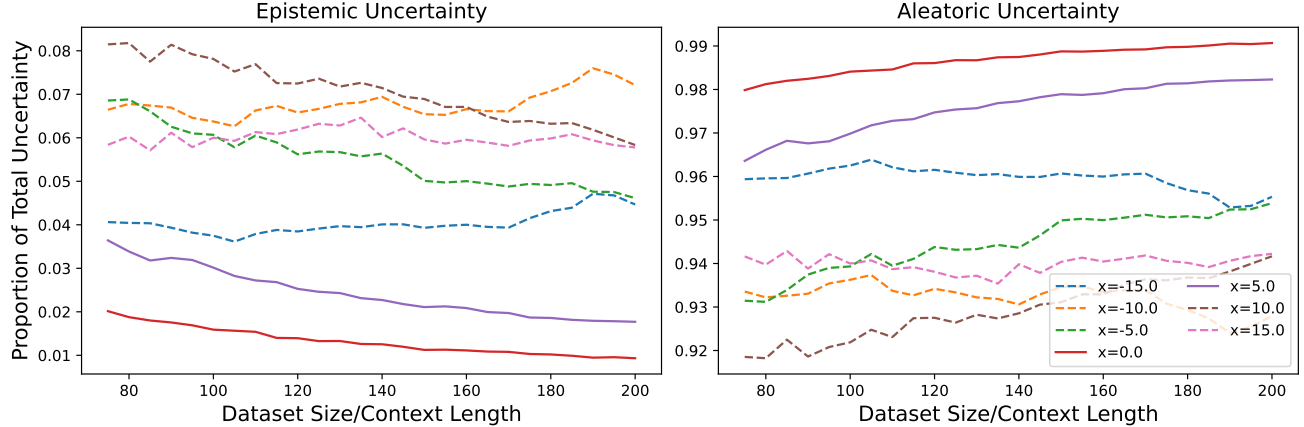


Figure 11. **Logistic regression (1D).** Proportion of the epistemic and aleatoric uncertainty for TabPFN with different test covariates x^* against varying dataset size. Solid and dotted lines indicated in-distribution and out-of-distribution x^* , respectively.

D.3. Three-class spirals

We generate a three-class spirals dataset in \mathbb{R}^2 with $C = 3$ arms. For class $c \in \{0, 1, 2\}$, we sample $t \sim \text{Uniform}(0, 1)$, set radius $r = 4.0 t$, and define the angle

$$\theta = 2\pi \cdot 2 \cdot t + \frac{2\pi c}{C}.$$

Points are generated as

$$x_1 = r \cos \theta + \varepsilon_1, \quad x_2 = r \sin \theta + \varepsilon_2,$$

with i.i.d. Gaussian noise $\varepsilon_1, \varepsilon_2 \sim \mathcal{N}(0, \sigma^2)$ using $\sigma = 0.1$. We sample $n = 200$ total points (approximately balanced across classes), randomly permute the dataset, and fix the random seed.

We evaluate uncertainty on a two-dimensional uniform grid over $x_1^* \in [-4.0, 4.0]$ and $x_2^* \in [-4.0, 4.0]$ with 100 points in each coordinate, and report heatmaps of total, aleatoric, and epistemic uncertainty over this region, see Figure 2.

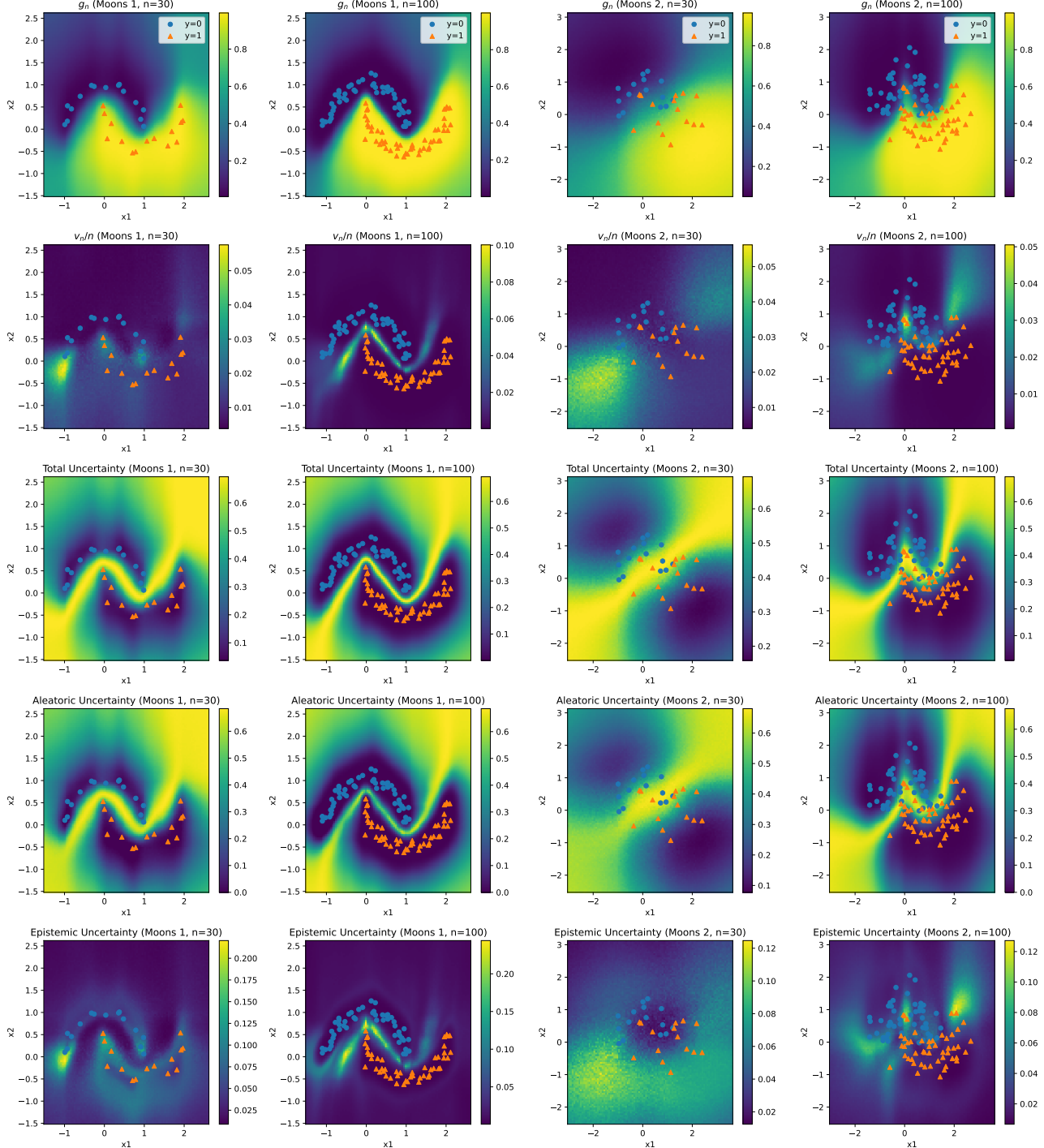


Figure 12. **Entropic uncertainty decomposition.** Rows (top to bottom): $g_n(x)$, $v_n(x)/n$, total uncertainty, aleatoric uncertainty, epistemic uncertainty. Columns (left to right): Moons 1 ($n = 30$), Moons 1 ($n = 100$), Moons 2 ($n = 30$), Moons 2 ($n = 100$).

E. Details on credible bands

Fix a grid $\mathbf{x} = [x_1, \dots, x_m]^T$. In binary classification we work with the success-probability vector

$$\mathbf{g}_n(\mathbf{x}) := (g_n(x_1), \dots, g_n(x_m))^T.$$

In regression, for a fixed threshold $t \in \mathbb{R}$, we work with the predictive CDF vector

$$\mathbf{F}_n(\mathbf{x}, t) := (F_n(x_1, t), \dots, F_n(x_m, t))^T.$$

Let $\widehat{\Sigma}_n$ denote the chosen plug-in covariance on the grid:

$$\widehat{\Sigma}_n \in \left\{ \frac{\mathbf{U}_n}{n}, \frac{\mathbf{V}_n}{n} \right\},$$

where the dependence on (\mathbf{x}, t) (regression) or on the classification setting is suppressed for readability. We approximate the expectation in \mathbf{U}_n using 1000 Monte Carlo samples. Let

$$s_j = \sqrt{\widehat{\Sigma}_{n,jj}}$$

denote the pointwise standard errors.

Pointwise $(1 - \alpha)$ credible intervals. For each grid point x_j , the pointwise $(1 - \alpha)$ credible interval is

$$\left[\mathbf{P}_{n,j} \pm z_{1-\alpha/2} s_j \right] \cap [0, 1],$$

where $\mathbf{P}_{n,j}$ denotes the j th component of $\mathbf{g}_n(\mathbf{x})$ (classification) or $\mathbf{F}_n(\mathbf{x}, t)$ (regression), and $z_{1-\alpha/2}$ is the $(1 - \alpha/2)$ -quantile of the standard normal distribution. The intersection enforces the natural range $[0, 1]$ for probabilities/CDF values.

Simultaneous sup- t $(1 - \alpha)$ credible band. We form a studentized sup-norm (sup- t) band (Olea & Plagborg-Møller, 2019). Draw

$$W^{(\ell)} \sim \mathcal{N}_m(0, \widehat{\Sigma}_n), \quad \ell = 1, \dots, L,$$

and compute

$$T^{(\ell)} := \max_{1 \leq j \leq m} \frac{|W_j^{(\ell)}|}{s_j}.$$

Let $c_{1-\alpha}$ be the empirical $(1 - \alpha)$ -quantile of $\{T^{(\ell)}\}_{\ell=1}^L$. The simultaneous sup- t $(1 - \alpha)$ credible band on the grid is

$$\left[\mathbf{P}_{n,j} \pm c_{1-\alpha} s_j \right] \cap [0, 1], \quad j = 1, \dots, m.$$

F. Frequentist coverage experiment details

F.1. Evaluation metrics

We assess the quality of the credible bands via their frequentist coverage rates. The target of the credible bands is the CDF or mass function of the true data-generating distribution. Specifically, for regression, this target is $f_0(x^*) = \Pr(Y \leq t | X = x^*)$ for a fixed t . For classification, it is $f_0(x^*) = \Pr(Y = 1 | X = x^*)$.

Let $C(x^*, z_{1:n})$ denote the credible set constructed from the dataset $z_{1:n}$ at a test covariate x^* . The credible bands are constructed over a grid \mathcal{X} consisting of 100 uniformly spaced points on $[-10, 10]$. The coverage calculation depends on the type of credible band. For pointwise credible bands, we compute the coverage frequency at each grid point x^* and then average over all points in \mathcal{X} :

$$\frac{1}{|\mathcal{X}|} \sum_{x^* \in \mathcal{X}} \frac{1}{R} \sum_{r=1}^R \mathbb{1}\{f_0(x^*) \in C(x^*, z_{1:n}^{(r)})\},$$

where coverage is evaluated over $R = 100$ independent draws of $z_{1:n}$ from the true data-generating process. For simultaneous credible bands, we compute the frequency with which the band covers the truth at all grid points in \mathcal{X} :

$$\frac{1}{R} \sum_{r=1}^R \mathbb{1} \left\{ \bigcap_{x^* \in \mathcal{X}} \left\{ f_0(x^*) \in C(x^*, z_{1:n}^{(r)}) \right\} \right\}.$$

In addition, we report the average width of the credible band, averaged over both repetitions and grid points:

$$\frac{1}{R} \sum_{r=1}^R \frac{1}{|\mathcal{X}|} \sum_{x^* \in \mathcal{X}} |C(x^*, z_{1:n}^{(r)})|.$$

All reported widths are averaged over the 100 repetitions.

F.2. Details on data generating process and rollouts

This section describes the data generating process (DGP) of Y given a univariate $X = x$. The sample of x are drawn from $\text{Uniform}(-10, 10)$. We use TabPFNClassifier with Probit and Categorical DGPs, and TabPFNRegressor for the remaining DGPs. We set $t = 0$ for all Gaussian DGPs, except for the Poisson case, where $t = 2$.

Linear (simple linear regression)

$$Y = 0.2X + \epsilon, \quad \epsilon \sim \mathcal{N}(0, 1).$$

Polynomial (polynomial regression)

$$Y = 1 - 0.03X^2 + \epsilon, \quad \epsilon \sim \mathcal{N}(0, 1).$$

Dependent (linear regression with dependent error)

$$Y \mid X \sim \mathcal{N}(0.5X + 1, \sigma^2(X)) \quad \text{where} \quad \sigma(x) = 0.5 + 0.5|x|.$$

Sine (sine wave with Gaussian noise)

$$Y = 0.5 \sin(X/2) + \epsilon, \quad \epsilon \sim \mathcal{N}(0, 0.5^2).$$

Poisson (Poisson regression)

$$Y \mid X \sim \text{Poisson}(\lambda(X)) \quad \text{where} \quad \lambda(x) = 0.05(x^2 - 80) + 5 = 0.05x^2 + 1.$$

Probit (probit regression)

$$Y \mid X \sim \text{Bernoulli}(p), \quad p = 0.6\Phi\left(\frac{x - 8}{4}\right) + 0.4\Phi\left(\frac{x + 8}{4}\right).$$

Categorical (multinomial logistic regression)

$$Y \mid X \sim \text{Categorical}(p_0, p_1, p_2, p_3), \quad p_j = \frac{\exp(z_j(x))}{\sum_{i=0}^3 \exp(z_i(x))}, \quad \text{for } j \in \{0, 1, 2, 3\},$$

where

$$z_0(x) = -\frac{(x + 5)^2}{10}, \quad z_1(x) = -\frac{x^2}{30}, \quad z_2(x) = -\frac{(x - 7)^2}{5}, \quad z_3(x) = -\frac{(x - 4)^2}{8}.$$

G. Proof preliminaries

G.1. A central limit theorem for quasi-martingales

Given a probability space $(\Omega, \mathcal{F}, \mathbb{P})$ and a Polish space S with its Borel sigma-algebra \mathcal{S} , a kernel on S is a function $K : \Omega \times \mathcal{S}$ satisfying:

- (i) for every $\omega \in \Omega$, $K(\omega, \cdot)$ is a probability measure on \mathcal{S} ;
- (ii) for each $B \in \mathcal{X}$, the function $K(\cdot, B)$ is measurable with respect to \mathcal{F} .

A Kernel K on \mathbb{R} is called a Gaussian kernel if $K(\omega, \cdot)$ is a Gaussian distribution with mean $\mu(\omega)$ and variance $\sigma^2(\omega)$, where μ and σ^2 are random variables defined on $(\Omega, \mathcal{F}, \mathbb{P})$. We denote the Gaussian kernel by $\mathcal{N}(\mu, \sigma^2)$ and interpret the Gaussian distribution with zero variance as the degenerate law centered on the mean.

Definition G.1. Let (M_n) be a sequence of random variables adapted to a filtration (\mathcal{G}_n) . For every $n \geq 0$, let K_n denote a regular version of the conditional distribution of M_{n+1} , given \mathcal{G}_n . If there exists a kernel K such that the sequence $(K_n(\omega, \cdot))_n$ converges weakly to $K(\omega, \cdot)$ for almost every $\omega \in \Omega$, then we say that the sequence (M_n) converges to K in the sense of almost-sure conditional convergence.

Definition G.2. A sequence (M_n) adapted to a filtration (\mathcal{G}_n) is called a quasi-martingale if

$$\sum_{n \geq 1} \mathbb{E}[|\mathbb{E}[M_{n+1} | \mathcal{G}_n] - M_n|] < +\infty.$$

A martingale is trivially a quasi-martingale since, for a martingale $|\mathbb{E}[M_{n+1} | \mathcal{G}_n] - M_n| = 0$. For a quasi-martingale, the expected absolute increment is not zero, but vanishes with n on average, faster than $1/n$.

Theorem G.3. If (M_n) is a quasi-martingale with respect to a filtration (\mathcal{G}_n) , and

$$\sup_n \mathbb{E}[|M_n|] < +\infty,$$

then M_n converges almost surely to a random limit M .

Next result provides a central limit theorem for quasi-martingales.

Theorem G.4 (Adapted from Proposition 1 in (Berti et al., 2011)). Let (M_n) be a sequence of real valued random variables adapted to the filtration $(\mathcal{G}_n)_{n \geq 0}$. Assume that (M_n) is uniformly integrable and that the following conditions hold:

- (i) $\sum_{n \geq 1} \sqrt{n} \mathbb{E}[|\mathbb{E}[M_n | \mathcal{G}_{n-1}] - M_{n-1}|] < +\infty$;
- (ii) $\mathbb{E}[\sup_{n \geq 1} \sqrt{n} |M_n - M_{n-1}|] < +\infty$;
- (iii) $n \sum_{k \geq n} (M_k - M_{k-1})^2 \rightarrow V$, \mathbb{P} -a.s.

Then there exists a random variable M such that M_n converges \mathbb{P} -a.s. to M , and

$$\mathcal{L}(\sqrt{n}(M_n - M) | \mathcal{G}_n) \rightarrow \mathcal{N}(0, V) \quad \mathbb{P}\text{-a.s.}$$

Remark. The proof of the theorem follows the same steps as the proof of Proposition 1 in (Berti et al., 2011). In that proposition, the authors assume that for every $n \geq 0$, $M_n = \mathbb{E}[Y_{n+1} | \mathcal{G}_n]$; however, a closer inspection of their argument shows that this assumption is never actually used.

Assumption (i) implies that (M_n) is a quasi martingale, since

$$\sum_{n \geq 1} \mathbb{E}[|\mathbb{E}[M_{n+1} | \mathcal{G}_n] - M_n|] \leq \sum_{n \geq 1} \sqrt{n} \mathbb{E}[|\mathbb{E}[M_n | \mathcal{G}_{n-1}] - M_{n-1}|] < +\infty.$$

Hence the convergence of M_n comes from the properties of uniformly integrable quasi-martingales.

The following result gives sufficient conditions for assumption (iii) in Theorem G.4.

Lemma G.5 (Lemma 2 in (Berti et al., 2011)). *Let (W_n) be a sequence of random variables adapted to a filtration (\mathcal{G}_n) . If the following conditions hold:*

- (i) $\sum_{n \geq 1} n^{-2} \mathbb{E}[W_n^2] < +\infty$;
- (ii) $\mathbb{E}[W_{n+1} | \mathcal{G}_n] \rightarrow W$, \mathbb{P} -a.s. for some random variable W ;

then

$$n \sum_{k \geq n} \frac{W_k}{k^2} \rightarrow W, \quad \frac{1}{n} \sum_{k=1}^n W_k \rightarrow W,$$

\mathbb{P} -a.s., as $n \rightarrow \infty$.

H. Proofs

H.1. Proof of Theorem 4.1

By (5), for every (x, t) , $F_n(x, t)$ is a uniformly bounded quasi-martingale. Therefore, it converges \mathbb{P} -a.s. (see Theorem G.3). It follows that, with probability one, $F_n(r, s)$ converges to a limit $H(r, s)$ for every r, s with rational coordinates. Fix ω such that the convergence holds. For simplicity of notation, we will omit ω in what follows. Fix x and let r'_n and r''_n be two sequences of rational numbers converging to x as $n \rightarrow \infty$. Fix $\epsilon > 0$ and let δ be such that

$$\sup_m |F_m(x, s) - F_m(z, s)| < \epsilon$$

for every z satisfying $\|z - x\| < \delta$. Let n_0 be such that for every $n \geq n_0$, $\|r'_n - x\| < \delta$ and $\|r''_n - x\| < \delta$. Then, for $n \geq n_0$,

$$\begin{aligned} |H(r'_n, s) - H(r''_n, s)| &\leq |H(r'_n, s) - F_m(r'_n, s)| + \sup_m |F_m(r'_n, s) - F_m(x, s)| \\ &\quad + \sup_m |F_m(x, s) - F_m(r''_n, s)| + |H(r''_n, s) - F_m(r''_n, s)| \\ &< 4\epsilon, \end{aligned}$$

for m large enough. Hence we can define for every $s \in \mathbb{Q}$ and every x

$$H(x, s) = \lim_n H(r_n, s)$$

where r_n is any sequence of points with rational coordinates converging to x as $n \rightarrow \infty$.

We now prove that $F_n(x, s)$ converges to $H(x, s)$, for every rational s and every x . We can write

$$\begin{aligned} &|F_n(x, s) - H(x, s)| \\ &\leq \sup_n |F_n(x, s) - F_n(r_m, s)| + |F_n(r_m, s) - H(r_m, s)| + |H(r_m, s) - H(x, s)| \\ &< 3\epsilon, \end{aligned}$$

if n and m are large enough. The function $H(x, s)$ is monotone non decreasing in $s \in \mathbb{Q}$ for every x . Indeed, we can write for any $s < t$, and any sequence (r_n) of point with rational coordinates converging to x ,

$$\begin{aligned} H(x, t) - H(x, s) &= \lim_n (H(r_n, t) - H(r_n, s)) \\ &= \lim_n \lim_m (F_m(r_n, t) - F_m(r_n, s)) \geq 0. \end{aligned}$$

We now define, for every x and t

$$H(x, t) = \inf_{s > t, s \in \mathbb{Q}} H(x, s)$$

The function $x \mapsto H(x, t)$ is measurable for every t . Moreover, for every x , $H(x, \cdot)$ is monotone non decreasing, and by assumption (i), it converges to 0 as $t \rightarrow -\infty$ and to 1 as $t \rightarrow +\infty$. We now show that it is continuous from the right. Fix t and $\epsilon > 0$ and let $s > t$ be such that

$$H(x, s) < H(x, t) + \epsilon.$$

Then for every $u \in (t, s)$

$$H(x, t) \leq H(x, u) \leq H(x, s) < H(x, t) + \epsilon,$$

which proves right-continuity at t . Thus, $H(x, \cdot)$ is a distribution function on \mathbb{R} for every x , and it is a measurable function of x for every t . It is therefore a kernel.

We now prove that, for every x , $F_n(x, \cdot)$ converges to $H(x, \cdot)$ weakly. Let t be a continuity point for $H(x, \cdot)$ and let $\epsilon > 0$. There exist $u < r < t < s$ with $s, r \in \mathbb{Q}$,

$$H(x, u) > H(x, t) - \epsilon, \quad H(x, s) < H(x, t) + \epsilon.$$

Then we can write

$$H(x, t) - \epsilon \leq H(x, u) \leq H(x, r) \leq H(x, t) \leq H(x, s) \leq H(x, t) + \epsilon.$$

Then

$$\liminf_n F_n(x, t) \geq \liminf_n F_n(x, r) \geq H(x, r) \geq H(x, t) - \epsilon,$$

$$\limsup_n F_n(x, t) \leq \limsup_n F_n(x, s) \leq H(x, s) \leq H(x, t) + \epsilon.$$

The convergence is a consequence of the arbitrariness of ϵ .

□

H.2. Proof of Theorem 4.2

Denote by \tilde{F}_x the random probability measure with distribution function $t \mapsto \tilde{F}(x, t)$. We prove the theorem by induction on k . By Theorem 4.1,

$$\mathbb{P}[Y_{n+1} \in dy_1 \mid Z_{1:n}, X_{n+1} = x_1] \rightarrow \tilde{F}_{x_1}(dy_1).$$

Now suppose that the claim is true for every $j \leq k-1$. By the conditional independence assumption (iv) and the induction hypothesis, we can write

$$\begin{aligned} \mathbb{P}[Y_{n+1} \in dy_1, \dots, Y_{n+k} \in dy_k \mid Z_{1:n}, X_{n+1:n+k} = x_{1:k}] \\ = \mathbb{P}[Y_{n+k} \in dy_k \mid Z_{1:n}, X_{n+1:n+k} = x_{1:k}, Y_{n+1:n+k-1} = y_{1:k-1}] \\ \times \mathbb{P}[Y_{n+1} \in dy_1, \dots, Y_{n+k-1} \in dy_{k-1} \mid Z_{1:n}, X_{n+1:n+k-1} = x_{1:k-1}] \longrightarrow \prod_{i=1}^k \tilde{F}_{x_i}(dy_i) \quad \mathbb{P}\text{-a.s.} \end{aligned}$$

□

H.3. Proof of Theorem 4.3

By assumption, for every $i = 1, \dots, m$, $F_n(x_i, t_i)$ converges to $\tilde{F}(x_i, t_i)$ on a set of probability one. In what follows, we work on this set, so that all subsequent statements hold almost surely.

Fix a vector $\mathbf{u} = [u_1, \dots, u_m]^T$ with $\|\mathbf{u}\| = 1$, and define for every $n \geq 1$ $M_n = \mathbf{u}^T \mathbf{F}_n(\mathbf{x}, \mathbf{t})$. Let \mathcal{G}_0 be the trivial sigma-algebra, and for every $n \geq 1$ let \mathcal{G}_n be the sigma-algebra generated by $Z_{1:n}$. The sequence (M_n) is uniformly integrable. Moreover,

$$\begin{aligned} \sum_{n \geq 1} \sqrt{n} \mathbb{E} [|\mathbb{E}[M_n \mid \mathcal{G}_{n-1}] - M_{n-1}|] &= \sum_{n \geq 1} \sqrt{n} \mathbb{E} [|\mathbf{u}^T \mathbb{E}[\Delta_n(\mathbf{x}, \mathbf{t}) \mid Z_{1:n}]|] \\ &\leq \sum_{i=1}^m \sum_{n \geq 1} \sqrt{n} \mathbb{E} [|\mathbb{E}[\Delta_n(x_i, t_i) \mid Z_{1:n}]|] < +\infty, \end{aligned}$$

and

$$\mathbb{E} \left[\sup_{n \geq 1} \sqrt{n} |M_n - M_{n-1}| \right] = \mathbb{E} \left[\sup_{n \geq 1} \sqrt{n} |\mathbf{u}^T \Delta_n(\mathbf{x}, \mathbf{t})| \right] \leq \sum_{i=1}^m \mathbb{E} \left[\sup_{n \geq 1} \sqrt{n} |\Delta_n(x_i, t_i)| \right] < +\infty$$

where the inequalities hold by assumptions (i) and (ii). Furthermore, by (iii)

$$n \sum_{k \geq n} (M_k - M_{k-1})^2 = n \sum_{k \geq n} \mathbf{u}^T \Delta_k(\mathbf{x}, \mathbf{t}) \Delta_k(\mathbf{x}, \mathbf{t})^T \mathbf{u} \rightarrow \mathbf{u}^T \mathbf{V}(\mathbf{x}, \mathbf{t}) \mathbf{u} \quad \mathbb{P}\text{-a.s.}$$

By Theorem G.4, $\mathcal{L}(\sqrt{n}(\mathbf{u}^T(\mathbf{F}_n(\mathbf{x}, \mathbf{t}) - \tilde{\mathbf{F}}(\mathbf{x}, \mathbf{t}))) \mid Z_{1:n}) \rightarrow \mathcal{N}(0, \mathbf{u}^T \mathbf{V}(\mathbf{x}, \mathbf{t}) \mathbf{u})$. Since \mathbf{u} is an arbitrary unit vector, the claim follows.

H.4. Proof of Theorem 4.4

Let \mathcal{G}_0 be the trivial sigma-algebra, and for every $n \geq 1$, let \mathcal{G}_n be the sigma-algebra generated by $Z_{1:n}$. Fix a vector $\mathbf{u} = [u_1, \dots, u_m]^T$ with $\|\mathbf{u}\| = 1$, and define $W_n = n^2 \mathbf{u}^T \Delta_n(\mathbf{x}, \mathbf{t}) \Delta_n(\mathbf{x}, \mathbf{t})^T \mathbf{u}$. Then

$$\sum_{n \geq 1} n^{-2} \mathbb{E}[W_n^2] = \sum_{n \geq 1} n^2 \mathbb{E}[(\mathbf{u}^T \Delta_n(\mathbf{x}, \mathbf{t}))^4] \leq m^4 \sum_{i=1}^m \sum_{n \geq 1} n^2 \mathbb{E}[\Delta_n^4(x_i, t_i)] < +\infty,$$

and

$$\mathbb{E}[W_{n+1} \mid \mathcal{G}_n] = (n+1)^2 \mathbb{E}[\mathbf{u}^T \Delta_{n+1}^2(\mathbf{x}, \mathbf{t}) \Delta_{n+1}^2(\mathbf{x}, \mathbf{t})^T \mathbf{u} \mid Z_{1:n}] \rightarrow \mathbf{u}^T \mathbf{V}(\mathbf{x}, \mathbf{t}) \mathbf{u} \quad \mathbb{P}\text{-a.s.},$$

by assumptions (i) and (ii). Then by Lemma G.5

$$n \sum_{k \geq n} \frac{W_k}{k^2} = n \sum_{k \geq n} \mathbf{u}^T \Delta_k(\mathbf{x}, \mathbf{t}) \Delta_k(\mathbf{x}, \mathbf{t})^T \mathbf{u} \rightarrow \mathbf{u}^T \mathbf{V}(\mathbf{x}, \mathbf{t}) \mathbf{u}$$

and

$$\frac{1}{n} \sum_{k=1}^n W_k = \frac{1}{n} \sum_{k=1}^n k^2 \mathbf{u}^T \Delta_k(\mathbf{x}, \mathbf{t}) \Delta_k(\mathbf{x}, \mathbf{t})^T \mathbf{u} \rightarrow \mathbf{u}^T \mathbf{V}(\mathbf{x}, \mathbf{t}) \mathbf{u}.$$

\mathbb{P} -a.s. Since \mathbf{u} is an arbitrary unit vector, the claim follows.

H.5. Proof of Theorem 4.5

Since \mathbf{U}_n and \mathbf{V}_n are functions of $Z_{1:n}$, then under the assumptions (i) and (ii) of Theorem 4.3 and (i), (ii) of Theorem 4.4, for every matrix \mathbf{S} and vector \mathbf{s}

$$\mathbb{E} \left[\exp(i\mathbf{S} \circ \mathbf{U}_n(\mathbf{x}, \mathbf{t}) + i\mathbf{s}^T \sqrt{n}(\mathbf{F}_n(\mathbf{x}, \mathbf{t}) - \tilde{\mathbf{F}}(\mathbf{x}, \mathbf{t}))) \mid Z_{1:n} \right] \rightarrow \exp \left(i\mathbf{S} \circ \mathbf{V}(\mathbf{x}, \mathbf{t}) - \frac{1}{2} \mathbf{s}^T \mathbf{V}(\mathbf{x}, \mathbf{t}) \mathbf{s} \right),$$

and

$$\mathbb{E} \left[\exp(i\mathbf{S} \circ \mathbf{V}_n(\mathbf{x}, \mathbf{t}) + i\mathbf{s}^T \sqrt{n}(\mathbf{F}_n(\mathbf{x}, \mathbf{t}) - \tilde{\mathbf{F}}(\mathbf{x}, \mathbf{t}))) \mid Z_{1:n} \right] \rightarrow \exp \left(i\mathbf{S} \circ \mathbf{V}(\mathbf{x}, \mathbf{t}) - \frac{1}{2} \mathbf{s}^T \mathbf{V}(\mathbf{x}, \mathbf{t}) \mathbf{s} \right),$$

where \circ denote Hadamard product of matrices and i is the imaginary unit. Hence, the conditional distribution of $(\mathbf{U}_n(\mathbf{x}, \mathbf{t}), \sqrt{n}(\mathbf{F}_n(\mathbf{x}, \mathbf{t}) - \tilde{\mathbf{F}}(\mathbf{x}, \mathbf{t})))$, given $Z_{1:n}$, converge to $\delta_{\mathbf{V}(\mathbf{x}, \mathbf{t})} \times \mathcal{N}_m(0, \mathbf{V}(\mathbf{x}, \mathbf{t}))$ \mathbb{P} -almost surely. The same conclusion applies to $(\mathbf{V}_n(\mathbf{x}, \mathbf{t}), \sqrt{n}(\mathbf{F}_n(\mathbf{x}, \mathbf{t}) - \tilde{\mathbf{F}}(\mathbf{x}, \mathbf{t})))$. If the matrix $\mathbf{V}(\mathbf{x}, \mathbf{t})$ is \mathbb{P} -a.s. positive definite, then $\mathbf{U}_n(\mathbf{x}, \mathbf{t})$ and $\mathbf{V}_n(\mathbf{x}, \mathbf{t})$ are also positive definite for all sufficiently large n . Thus we obtain the claim. 4.5.

I. Additional real data illustration

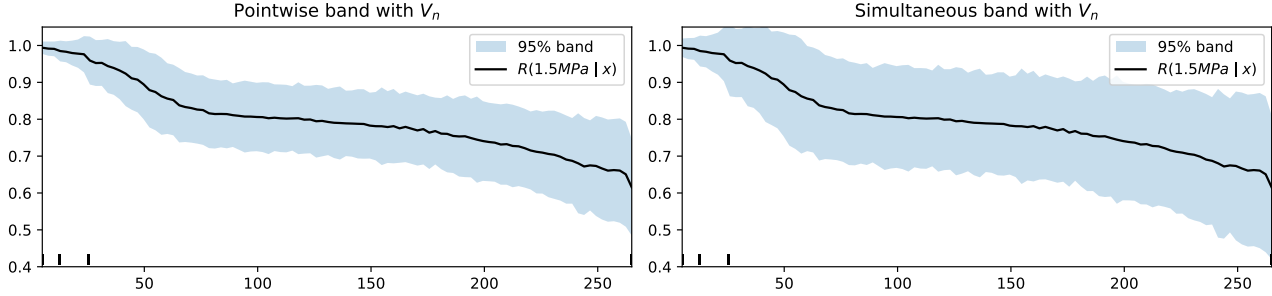


Figure 13. **Left:** pointwise 95% credible band for TabPFN predicted conditional reliability $R(1.5 \text{ MPa} | x)$. **Right:** simultaneous 95% credible band TabPFN predicted conditional reliability $R(1.5 \text{ MPa} | x)$. The result is comparable to that obtained in Fig. 7.10 in Hamada et al. (2008) which shows length (mm) versus posterior mean and 0.05/0.95 quantiles of the conditional reliability $R(1.5 \text{ MPa} | x)$.

Following *Bayesian Reliability* (Hamada, Wilson, Reese, and Martz, 2008, Ex. 7.4), we analyze tensile strengths (MPa) of silicon–carbide fibers tested at four gauge lengths $x \in \{5.0, 12.7, 25.4, 265\}$ mm. The sample size of this dataset is $n = 214$. Let S denote fiber strength and x the gauge length. The textbook models the conditional distribution

$$S | x \sim \text{Weibull}(\lambda(x), \beta(x)), \log \lambda(x) = \gamma_1 + \gamma_2 \log x, \log \beta(x) = \gamma_3 + \gamma_4 \log x,$$

with independent diffuse Normal priors on $\gamma_{1:4}$. The target is the *conditional exceedance (reliability) probability* at strength threshold s ,

$$R(s | x) = \Pr(S > s | x) = \exp\left(-\lambda(x) s^{\beta(x)}\right) = \exp\left(-e^{\gamma_1} x^{\gamma_2} s^{e^{\gamma_3} x^{\gamma_4}}\right).$$

The traditional Bayesian workflow, which the textbook illustrates, is to first obtain posterior draws $\{\gamma^{(m)}\}_{m=1}^M$ via MCMC. For a grid of lengths $\mathcal{X} = \{x_1, \dots, x_G\}$ and fixed threshold $s = 1.5 \text{ MPa}$, they evaluate

$$R^{(m)}(s | x_g) = \exp\left(-e^{\gamma_1^{(m)}} x_g^{\gamma_2^{(m)}} s^{e^{\gamma_3^{(m)}} x_g^{\gamma_4^{(m)}}}\right), g = 1, \dots, G.$$

At each x_g , one can summarize $\{R^{(m)}(s | x_g)\}_{m=1}^M$ by its posterior mean (solid curve) and the 0.05 and 0.95 posterior quantiles (dashed curves). Fig. 7.10 in Hamada et al. (2008) show that reliability decreases with increasing length, and uncertainty widens slightly as x grows.

We produce an analog analysis to Fig. 7.10 in Hamada et al. (2008) using TabPFN and our predictive CLT. The result is in Figure 13.

J. Gap experiments

We illustrate credible bands constructed using the predictive CLT in Figure 14-20. We use the DGPs and rollouts listed in Appendix F.2, except that half of the x samples are drawn from $\text{Uniform}(-8, -2)$ and the other half from $\text{Uniform}(2, 8)$. For each DGP, we consider three sample sizes ($n = 200$, $n = 500$, and $n = 1000$). Details of the credible band construction are provided in Appendix E.

Overall, the credible bands provide good coverage of the true probability $f_0(x)$, as defined in Appendix F.1. Bands constructed with \mathbf{V}_n are tighter than those based on \mathbf{U}_n , and the bands become tighter as n increases. The \mathbf{U}_n bands appear jagged due to Monte Carlo error in approximating the expectation in \mathbf{U}_n .

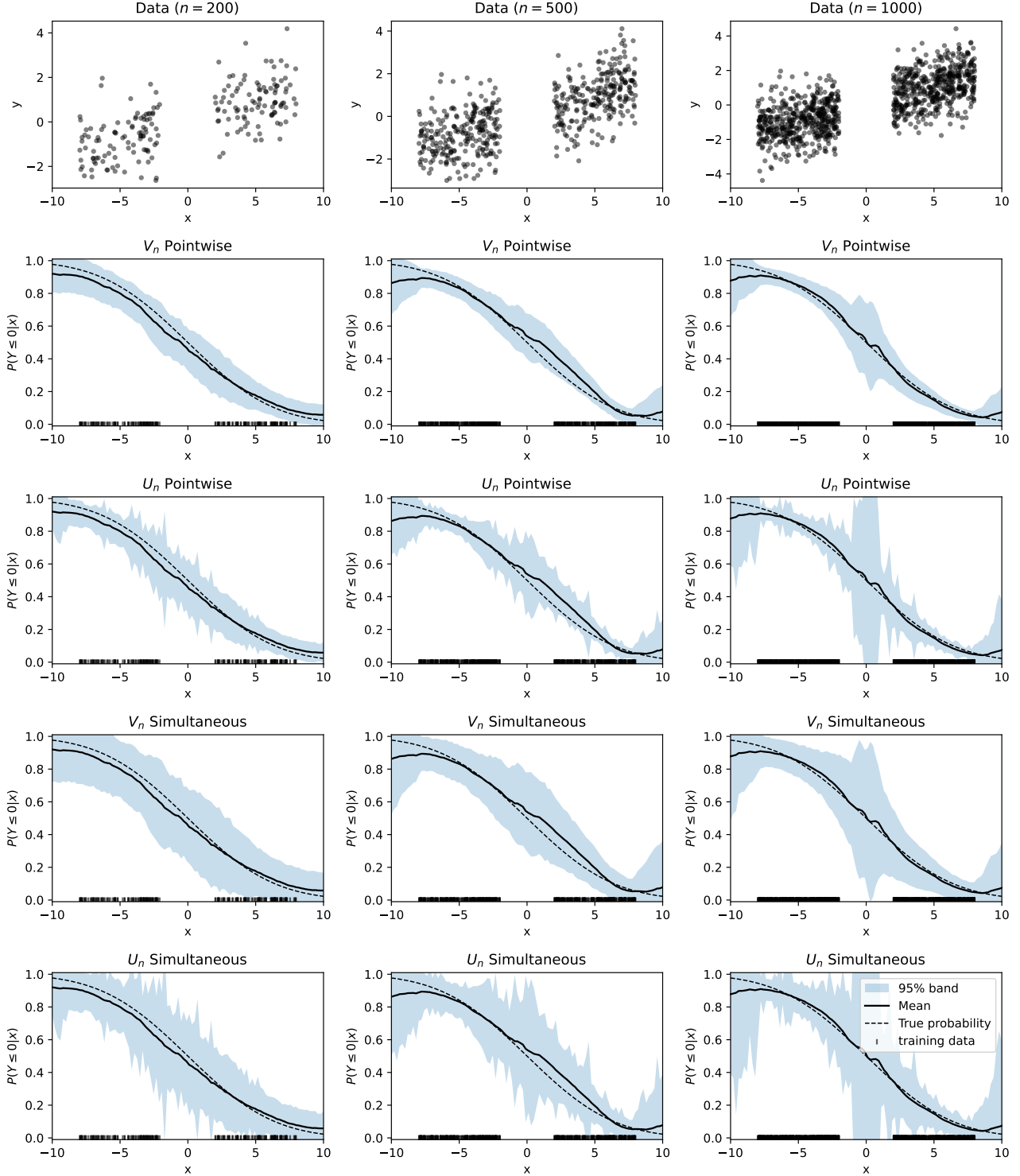


Figure 14. Credible bands with the Linear DGP under different combinations of construction methods (pointwise and simultaneous) and covariance estimators (\mathbf{V}_n and \mathbf{U}_n), with a gap in observations between -2 and 2 . Each column corresponds to a different sample size n . The first row shows the sampled dataset, and the subsequent rows show the corresponding credible bands. The observed x values are marked in the credible band plots.

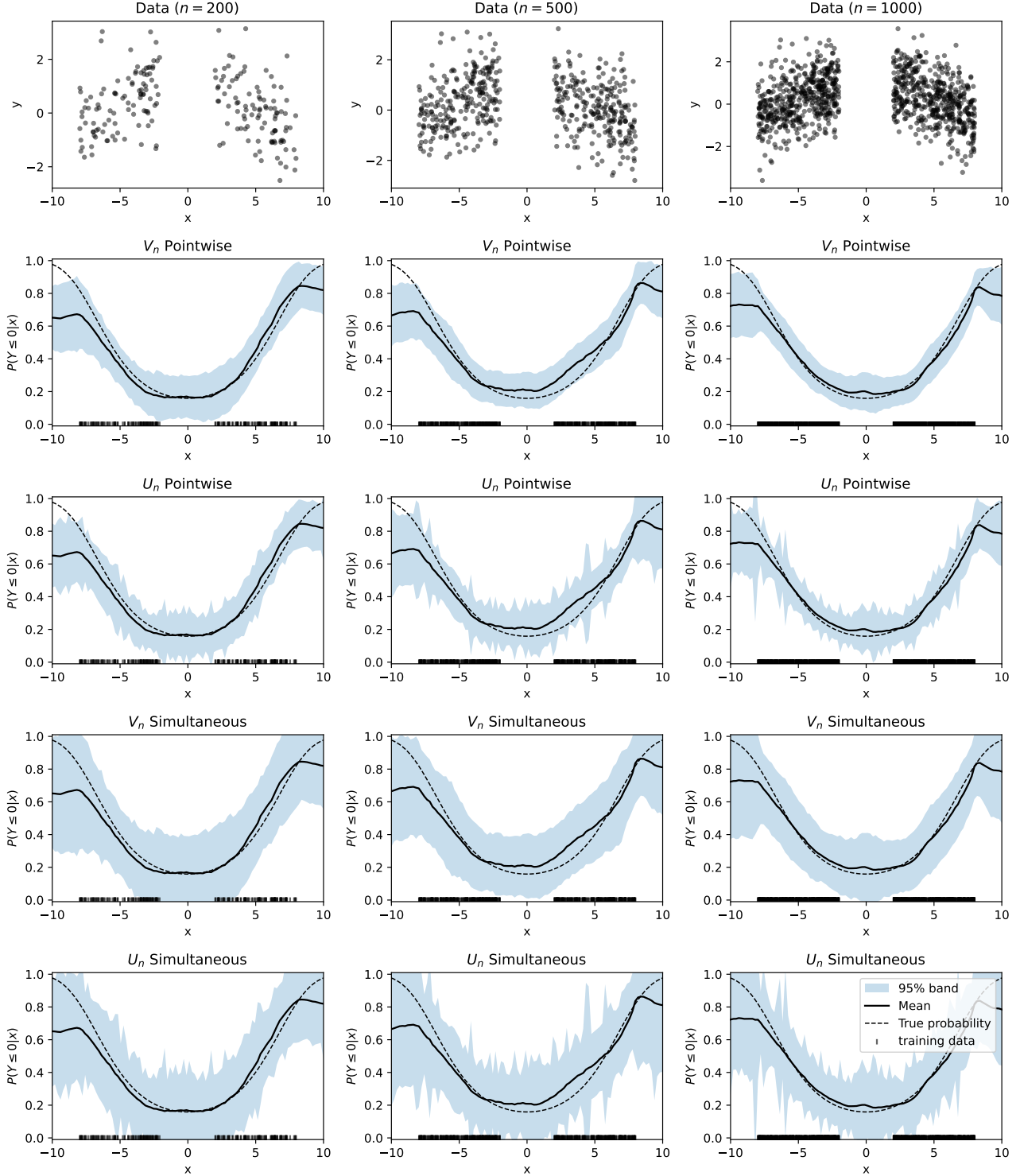


Figure 15. Credible bands with the Polynomial DGP under different combinations of construction methods (pointwise and simultaneous) and covariance estimators (\mathbf{V}_n and \mathbf{U}_n), with a gap in observations between -2 and 2 . Each column corresponds to a different sample size n . The first row shows the sampled dataset, and the subsequent rows show the corresponding credible bands. The observed x values are marked in the credible band plots.

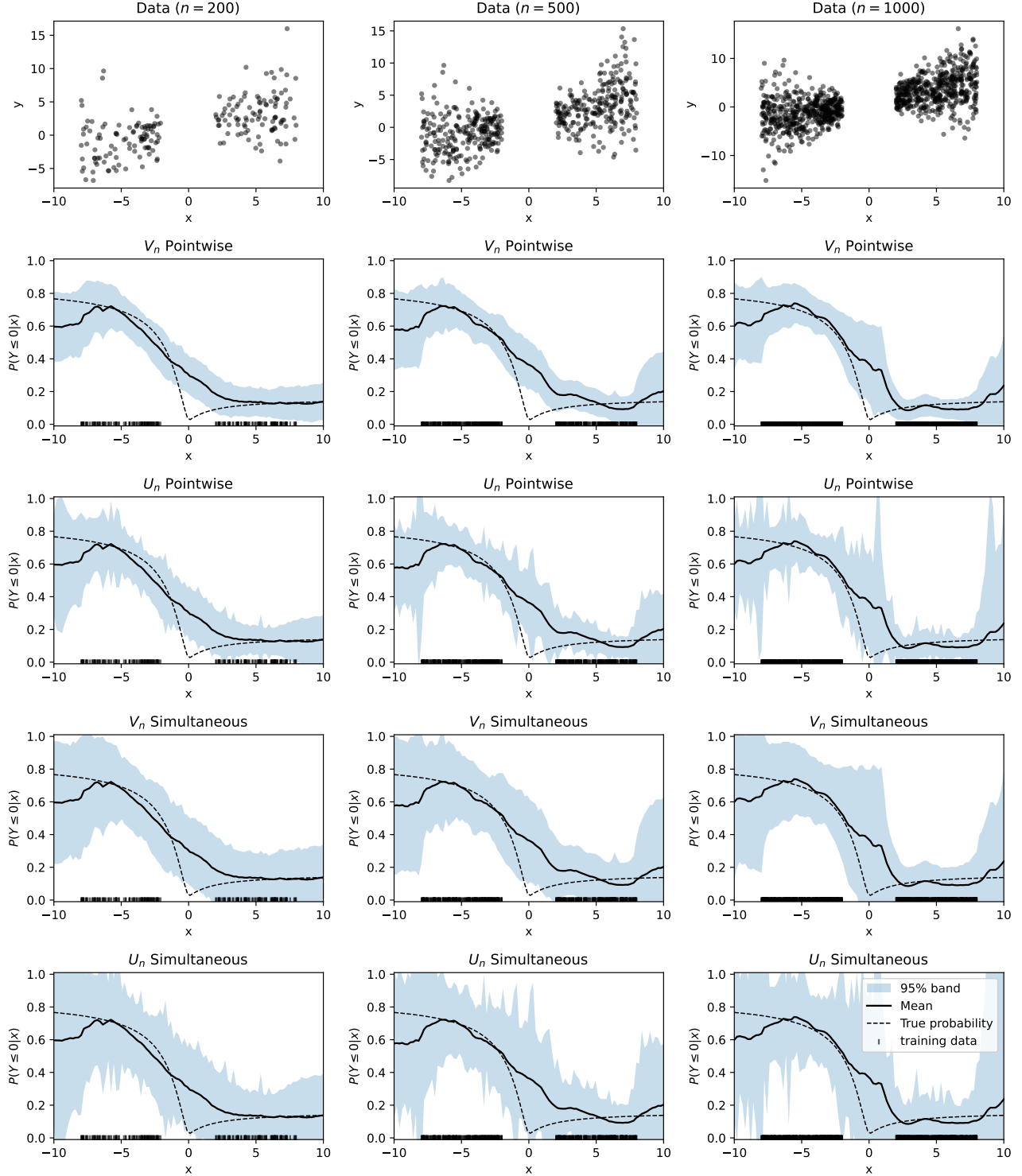


Figure 16. Credible bands with the Dependent DGP under different combinations of construction methods (pointwise and simultaneous) and covariance estimators (\mathbf{V}_n and \mathbf{U}_n), with a gap in observations between -2 and 2 . Each column corresponds to a different sample size n . The first row shows the sampled dataset, and the subsequent rows show the corresponding credible bands. The observed x values are marked in the credible band plots.

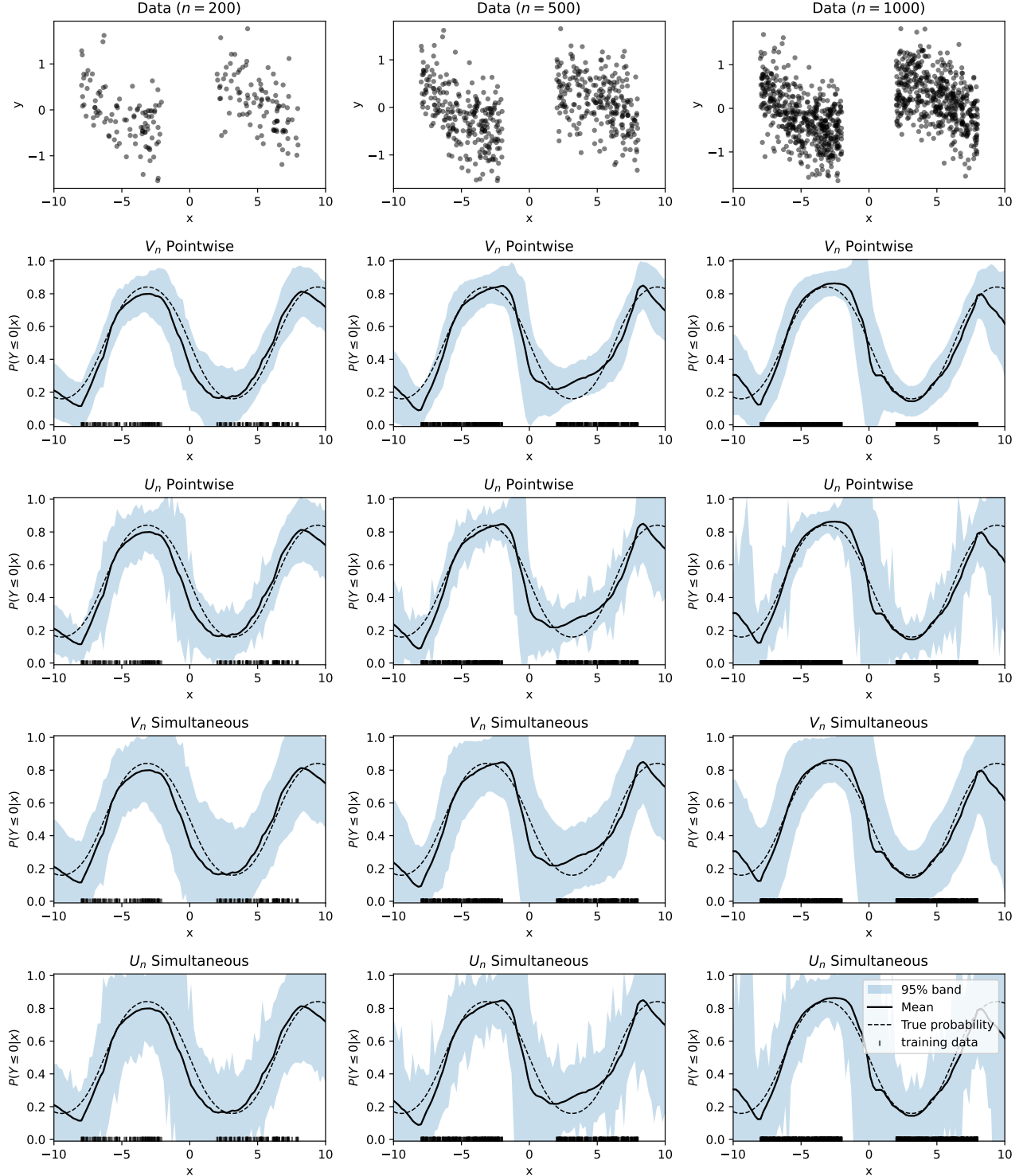


Figure 17. Credible bands with the Sine DGP under different combinations of construction methods (pointwise and simultaneous) and covariance estimators (\mathbf{V}_n and \mathbf{U}_n), with a gap in observations between -2 and 2 . Each column corresponds to a different sample size n . The first row shows the sampled dataset, and the subsequent rows show the corresponding credible bands. The observed x values are marked in the credible band plots.

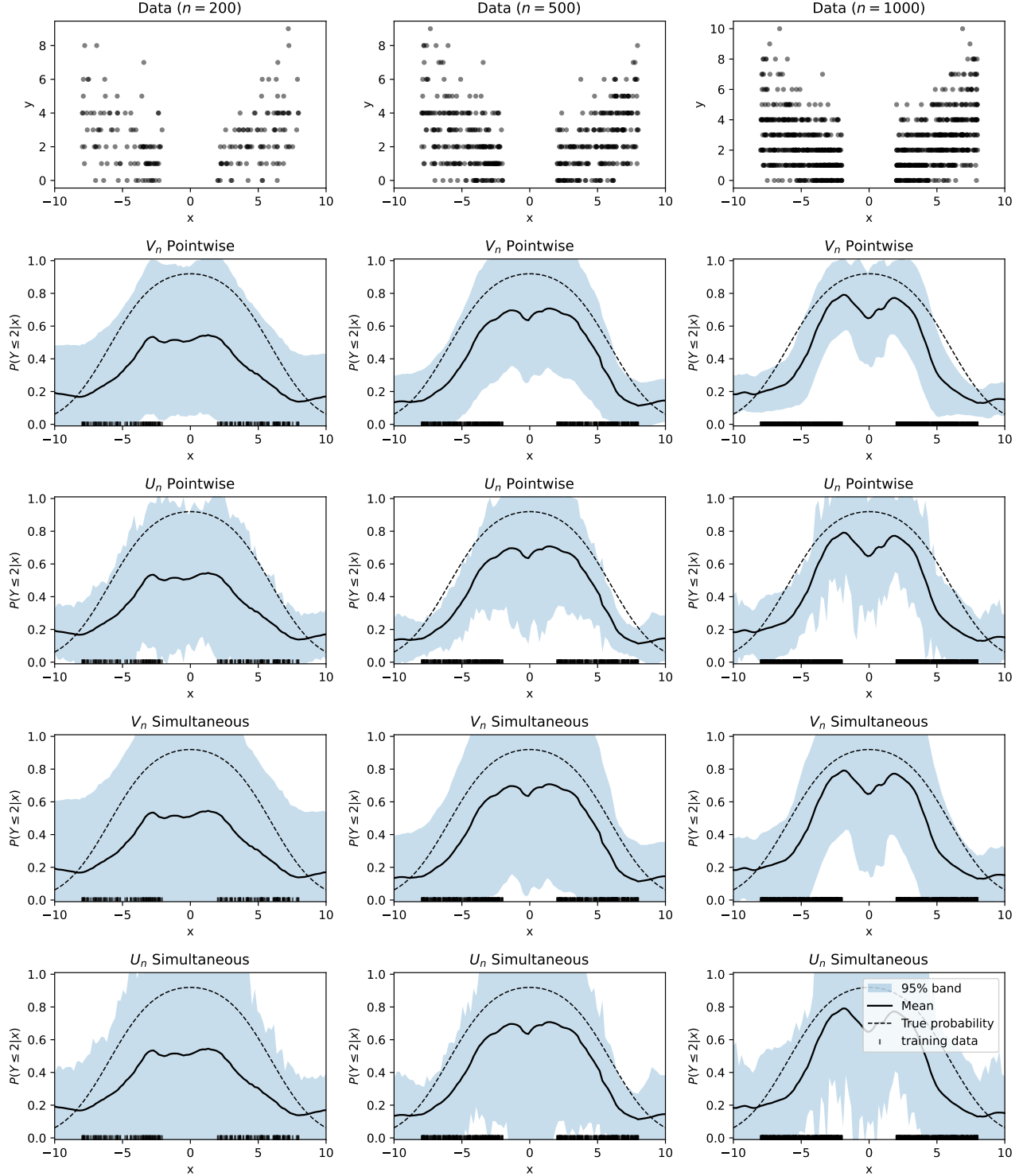


Figure 18. Credible bands with the Poisson DGP under different combinations of construction methods (pointwise and simultaneous) and covariance estimators (\mathbf{V}_n and \mathbf{U}_n), with a gap in observations between -2 and 2 . Each column corresponds to a different sample size n . The first row shows the sampled dataset, and the subsequent rows show the corresponding credible bands. The observed x values are marked in the credible band plots.

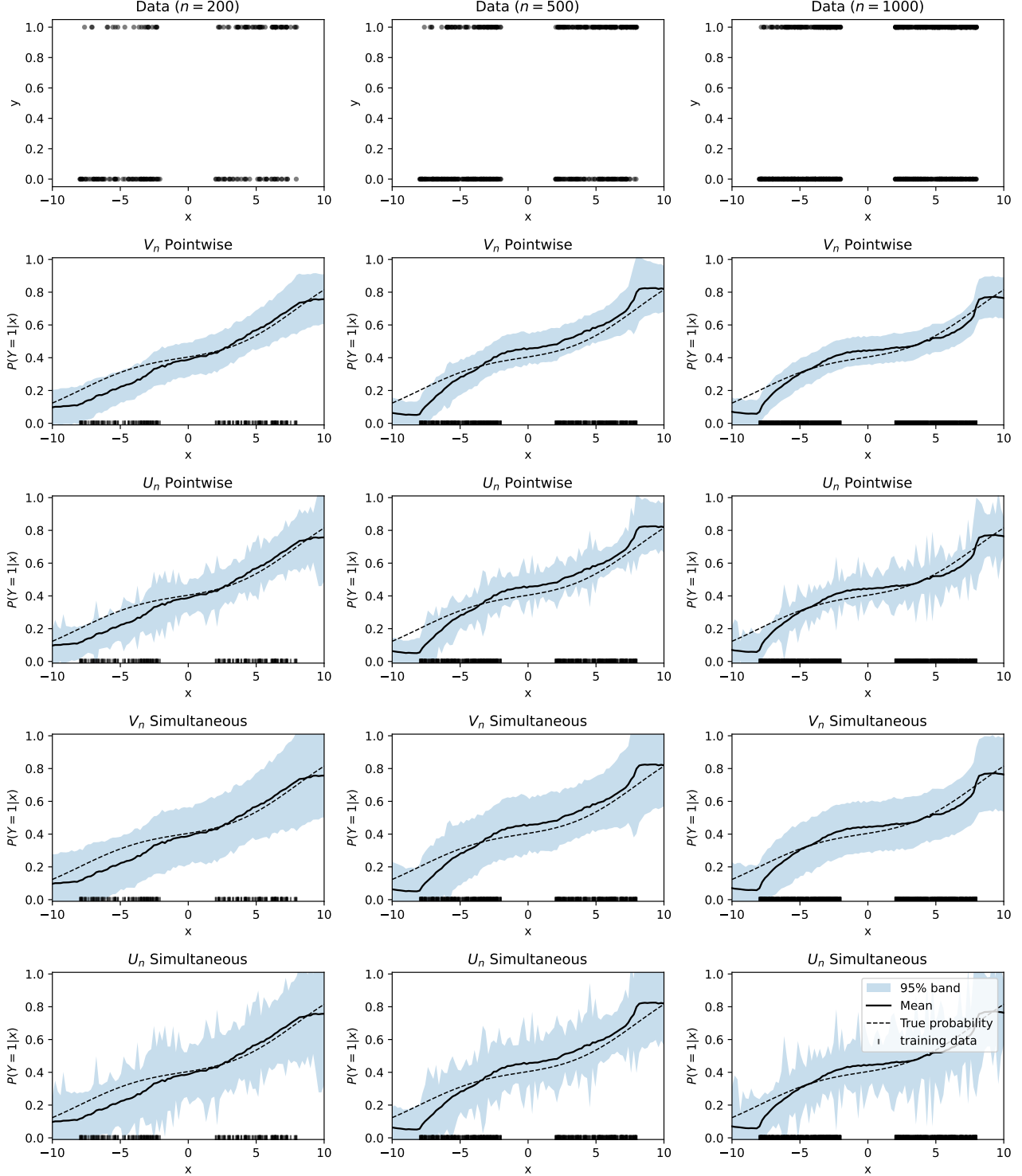


Figure 19. Credible bands with the Probit DGP under different combinations of construction methods (pointwise and simultaneous) and covariance estimators (\mathbf{V}_n and \mathbf{U}_n), with a gap in observations between -2 and 2 . Each column corresponds to a different sample size n . The first row shows the sampled dataset, and the subsequent rows show the corresponding credible bands. The observed x values are marked in the credible band plots.

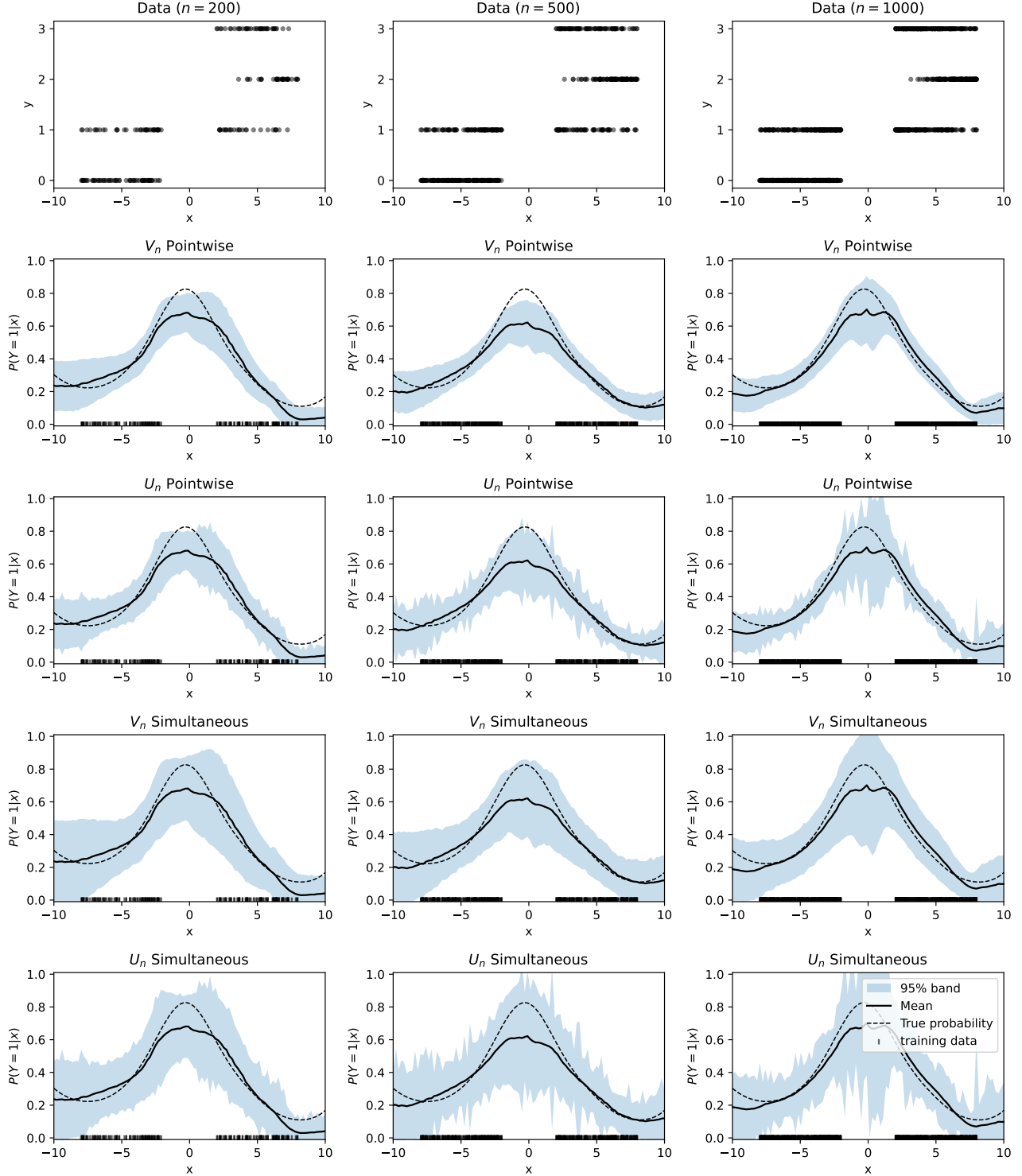


Figure 20. Credible bands with the Categorical DGP under different combinations of construction methods (pointwise and simultaneous) and covariance estimators (\mathbf{V}_n and \mathbf{U}_n), with a gap in observations between -2 and 2 . Each column corresponds to a different sample size n . The first row shows the sampled dataset, and the subsequent rows show the corresponding credible bands. The observed x values are marked in the credible band plots.